CHAPTER VII

MULTISTEP REACTIONS

1. INTRODUCTION

The DWA as used in Chapter V and Section VI.3 describes a single-step reaction as exhibited by the explicit appearance of the responsible interaction only once in the transition matrix element [see (V.4.8) and (VI.2.26′)]. More picturesquely, one visualizes the incident projectile passing near the target and exciting the latter or transferring a particle to it and then departing without further exchange of energy or mass. Clearly, it is possible that more than one interaction can occur before the final state is achieved. For example, in the case of a particle transfer reaction to the ground state of the residual nucleus, the particle may be transferred to form an excited state of the residual nucleus, which upon a second interaction makes a transition to its ground state. Or in the case of elastic scattering of a deuteron, one step might involve the transfer of the deuteron's neutron to the target, followed by the second step, in which the neutron is emitted and combines with the proton to reform the deuteron. Both of these examples are *two-step reactions*. The reader can devise other examples of two-step reactions or indeed, reactions involving many steps. One refers to this class as *multistep* (direct) *reactions*. In this chapter we develop the theoretical framework in which these reactions can be studied.

When will the multistep process be important? Certainly, when the single-step reaction cross section is abnormally reduced, as occurs for production at large angles, for large energy loss, and for large angular and linear momentum transfers. It may occur because of poor overlap between the initial and final wave functions (because of poor momentum matching) for deformed nuclei if a considerable change in shape were to occur. On the other hand, there may be specially favored transitions to intermediate states that can serve as doorway

states en route to the final state. Two reactions we refer to later in this chapter may serve as examples. The excitation of the 4_1^+ state of a vibrational nucleus can be accomplished by either a single step induced by a fourth-order multipole or by two quadrupole steps proceeding therefore through a 2_1^+ intermediate state. The amplitude for these steps are comparable. In the transfer (p, t) reaction, the ground state-to-ground state reaction is favored in superconducting nuclei. In considering the excitation of the 2^+ level by this reaction, one must include not only the single-step but also the two-step reaction, in which the first step is ground state-to-ground state transition, followed by an inelastic excitation. Or the inelastic excitation can occur in the target nucleus and the transfer to the excited state of the final nucleus follows.

As the change from the initial nuclear structure increases, more steps may become important. However, the number of steps is limited since the probability for an individual step is less than unity. At higher energies, the probability for any single step is much reduced, with the consequence that at sufficiently high energy the single-step approximation suffices.

On the other hand, at sufficiently low energies the incident projectile may lose so much energy to the target nucleus that it becomes trapped and eventually fuses with the target to form a compound nucleus. Reemission of the projectile or other particles now occurs through an evaporation-like process, as described in Chapter IV. Of course, if the energy is high enough, the system may emit before the compound nucleus is formed; this process is referred to as *precompound reaction.* After a number of steps, precompound emission becomes improbable and the compound nucleus is formed. In this book we use the term *statistical multistep compound reaction* to describe both the precompound emission and the formation of the compound nucleus.

Of course, in a given reaction, all of the reaction types discussed above can occur; that is, the reaction can be single-step and multi-step direct. It can lead to the formation of a compound nucleus, or it can terminate before the compound nucleus is formed, as in the multistep compound reaction just discussed. These possibilities are reflected in the spectrum of a given reaction product at a given emission angle. A typical spectrum fo a (p, n) reaction is illustrated in Fig. 1.1, where the double differential cross section for the production of a neutron at an energy E_n and at angle ϑ_0 is plotted as a function of neutron energy. The incident proton has an energy of some tens of MeV. As indicated in the figure, each of the processes discussed above dominates a particular spectral region. This is a qualitative rather than a quantitative association. But by and large, the excitation of individual low-lying energy levels in the residual nucleus proceeds via the single-step direct process. On the other hand, the low-energy slow neutrons are for the most part produced after the target nucleus and incident proton combine to form a compound nucleus. As one goes away from the extremes, the multistep processes become dominant. On the low-energy end, emission before the compound nucleus is fully developed takes place, while at the high-energy end, the increased energy loss to the target is more readily obtained in several steps than in one. In the intermediate region

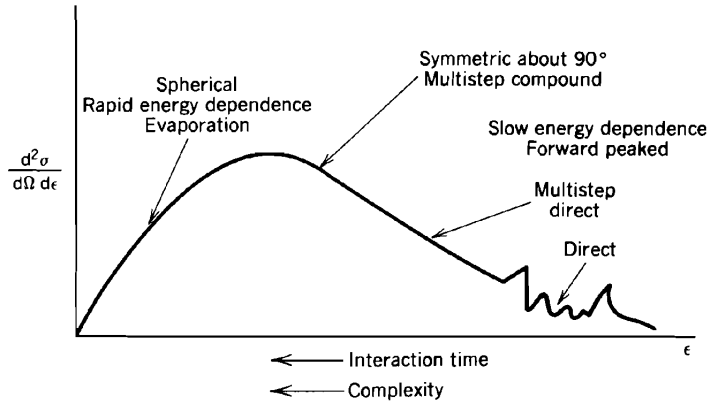

FIG. 1.1. Neutron energy (E) spectrum of an angle $\vartheta = \vartheta_0$.

far from the extremes, both the multistep direct and compound reactions play equally important roles.

With a change in the angle ϑ_0, the relative emphasis on the various processes changes. At forward angles the single direct process will dominate and there will be relatively little cross section in the low-energy part of the spectrum. At large angles, the multistep direct process will be important for relatively high neutron energies, while the evaporation and multistep compound reactions will dominate the low-energy end of the spectrum.

At low energies of the incident projectile, one can expect that the compound and multistep compound reactions will dominate since it will be relatively easy for the projectile and target to fuse after relatively few steps. However, as the projectile energy increases, the direct processes becomes increasingly important and eventually make the major contribution to the cross section.

Increasing E_n in Fig. 1.1 maps qualitatively into decreasing interaction time. For large E_n, the angular distribution is forward peaked, while variation of the cross section with projectile energy is slow. Both features are characteristic of a short interaction time (i.e., the time during which the projectile and target interact). The slow energy dependence, using the Heisenberg uncertainty relation, directly indicates short interaction times. The forward peaking corroborates this result since the information indicating the incident direction is preserved. For small E_n the angular distribution in the evaporation region is spherical, indicating complete loss of information regarding the incident direction and therefore a long interaction time. As one moves into the multistep compound domain, the angular distribution is symmetric about 90° but is definitely anisotropic. The variation in cross section with energy is rapid (see the discussion of Ericson fluctuations in Chapter IV), demonstrating that the interaction time is relatively long.

One anticipates that a longer interaction time indicates a greater number of steps. Moreover, an increasing number of steps correlates with increasing complexity of the wave function. These correlations are indicated in Fig. 1.1.

This sketch of the emitted spectrum omits the influence of special features such as giant resonances. This depends critically on the nature of the interference between the resonant and nonresonant amplitudes. If the excitation energy is sufficiently high, so that many levels in the residual nucleus can be excited, it is anticipated that on averaging over these levels, the interference term will average to zero. Then the cross section will be a sum of the cross sections for the resonant and for nonresonant processes.

The formal treatment of multistep direct processes can proceed by evaluating the transition matrix to nth order in the coupling potential v, where n is the number of steps. For example, for a three-step process,

$$\mathcal{T}_{fi} = \langle \phi_f^{(-)} v \phi_i^{(+)} \rangle + \left\langle \phi_f^{(-)} v \frac{1}{E^{(+)} - H} v \phi_i^{(+)} \right\rangle + \left\langle \phi_f^{(-)} v \frac{1}{E^{(+)} - H} v \frac{1}{E^{+} - H} v \phi_i^{(+)} \right\rangle + \cdots \tag{1.1}$$

where $\phi_i^{(+)}$ and $\phi_f^{(+)}$ are the initial and final wave functions, $1/(E^{(+)} - H)$ is the intermediate-state propagator, and H is the intermediate-state Hamiltonian. The spectral decomposition of $1/(E^{(+)} - H)$ provides various possibilities for intermediate states. The first term in (1.1) is the single-step,the second term the two-step, and the last term the three-step amplitude. We discuss later how these terms might be evaluated.

Equation (1.1) is adequate if v is relatively weak but fails if the coupling is strong. This is, in fact, the case when the low-lying collective states are involved, for then a particular multipole moment (e.g., the quadrupole) of the coupling potential can produce, with substantial probability, a particular member of the band of collective states. As a consequence, iterations of the coupling can be appreciable. Moreover, because of the close relation of the collective states to each other, there can be phase relations among the various multistep amplitudes that will lead to significant interference effects. An expansion like (1.1) is not useful under these circumstances.

Instead, one must put all of these excitations and the ground state on a more-or-less equal footing. Toward this end, one employs the *multichannel* optical model described in Chapter V [Eqs. (8.5), (8.6), and (8.7)], which takes the form

$$(E - H_{\text{eff}})P\Psi = 0 \tag{1.2}$$

where P projects on to all the channels of interest. H_{eff} contains the effects of the omitted channels, usually energy averaged, so that H_{eff} is an optical model Hamiltonian. One must be careful to distinguish if from the *single-channel*

optical model of Chapter V. In the first place, H_{eff} involves explicitly more than one channel, whereas the single-channel optical model deals only with the elastic channel; the effects of all the other channels are contained in the single-channel optical model Hamiltonian. As a consequence, the magnitude of the absorptive component of the single-channel optical Hamiltonian will be larger (often, substantially) than the absorptive component of H_{eff}.

Upon expressing $P\Psi$ in terms of the channels included in P, (1.1) becomes a set of coupled Schrödinger equations. The steps of which we spoke earlier are generated by the coupling between the channels. In principle, one can proceed by solving these equations exactly, a procedure that is practical only if the number of these equations is not too large. On the other hand, when the number of coupled channels is large, statistical methods can be employed. The resulting process is referred to as the *statistical multistep direct reaction.* There are in-between situations in which the coupling among some special channels has to be treated exactly, while statistical methods will suffice for the remainder.

In summary, the multistep direct reactions can be treated using (1) higher-order DWA, (2) through the use of coupled channels, and finally (3) when the number of channels becomes large by using the statistical multistep direct theory. As remarked earlier, a discussion of the formation of the compound nucleus, including the precompound emission, will lead to the theory described as the statistical multistep compound reaction.

2. COUPLED CHANNELS AND HIGHER-ORDER DWA[‡]

It is convenient to combine the discussion of the coupled-channel method and the higher-order DWA, which is a particular approximation to the results obtained using the coupled-channel method. Moreover, at the start, for reasons of simplicity, we shall be concerned only with inelastic scattering, in which the target nucleus is excited by the incident projectile. It will be again assumed, for simplicity that the multistep process involves only excited states of the target. The Pauli principle required if the projectile is composed of nucleons will also be disregarded in this discussion. (See Section III.5, for a rigorous treatment.)

To obtain the coupled-channel equations, expand $P\Psi$ of (1.2) into the finite series

$$P\Psi = \sum_i \phi_i(0)\psi_i(1, 2, \ldots) \tag{2.1}$$

where ψ_i are the wave functions describing the ground and excited states of the target, while ϕ_i depends on the coordinates of the projectile relative to the center of mass of the target nucleus. The optical model Hamiltonian H_{eff} is the sum of the target Hamiltonian H_t, the kinetic energy operator T giving the

[‡]Tamura (65, 74); Satchler (83).

relative motion of the projectile–target nucleus system and the interaction $V^{(pt)}$ between the projectile and the target:

$$H_{\text{eff}} = H_t + T + V^{(pt)} \tag{2.2}$$

The wave functions ψ_i satisfy the equations

$$\begin{aligned} H_t\psi_i &= \varepsilon_i\psi_i \\ \langle\psi_i|\psi_j\rangle &= \delta_{ij} \end{aligned} \tag{2.3}$$

Inserting (2.1) into (1.2), one obtains

$$[E - \varepsilon_i - T - \langle\psi_i|V^{(pt)}\psi_i\rangle]\phi_i = \sum_{j\neq i}\langle\psi_i|V^{(pt)}\psi_j\rangle\phi_j \tag{2.4}$$

These equations are to be solved subject to the boundary conditions at infinity. These are (1) that except for the incident channel (target nucleus in the ground state), all the ϕ_i behave as $e^{ik_i r_0}/r_0$ where $k_i = [(2\mu/\hbar^2)(E-\varepsilon_i)]^{1/2}$ as $r_0 \to \infty$; (2) the incident channel wave function consists of a plane wave plus an outgoing wave in the same limit.

The first-order DWA for the excitation of the state ψ_a is obtained if one assumes that ϕ_a couples only to the incident channel ϕ_0, whose coupling to ϕ_a is neglected:

$$\begin{aligned} (E - \varepsilon_0 - T - V_{00})\phi_0 &= 0 \\ (E - \varepsilon_a - T - V_{aa})\phi_a &= V_{a0}\phi_0 \end{aligned} \tag{2.5}$$

where we have adopted the notation

$$V_{ab} \equiv \langle\phi_a|V^{(pt)}|\phi_b\rangle$$

The second-order DWA is obtained if one assumes that ϕ_a couples to the other states ϕ_b, which, however, couple only to the incident channel:

$$\begin{aligned} (E - \varepsilon_0 - T - V_{00})\phi_0 &= 0 \\ (E - \varepsilon_b - T - V_{bb})\phi_b &= V_{b0}\phi_0 \end{aligned} \tag{2.6a}$$

or

$$\phi_b = \frac{1}{E^{(+)} - \varepsilon_b - T - V_{bb}} V_{b0}\phi_0 \tag{2.6b}$$

The equation for ϕ_a is

$$(E - \varepsilon_a - T - V_{aa})\phi_a = V_{a0}\phi_0 + \sum_{b\neq a} V_{ab}\phi_b \tag{2.7}$$

Substituting for ϕ_b from (2.6), one obtains

$$(E - \varepsilon_a - T - V_{aa})\phi_a = V_{a0}\phi_0 + \sum_{b \neq a} V_{ab} \frac{1}{E^{(+)} - \varepsilon_b - T - V_{bb}} V_{b0}\phi_0 \tag{2.8}$$

The transition matrix is then

$$\mathcal{T}_{a0} \simeq \langle \phi_{a,0}^{(-)} | V_{a0}\phi_0^{(+)} \rangle + \sum_{b \neq a} \left\langle \phi_{a,0}^{(-)} \middle| \left[V_{ab} \frac{1}{E^{(+)} - \varepsilon_b - T - V_{bb}} V_{b0} \right] \phi_0^{(+)} \right\rangle \tag{2.9}$$

where

$$(E - \varepsilon_a - T - V_{aa})\phi_{a,0}^{(-)} = 0$$

The first term is the first-order DWA,, while the second is the second-order DWA and is in the form given by (1.1). One can evaluate the second-order DWA directly from (2.9), but in practice it is simpler to numerically integrate the equation for ϕ_o, then solve (2.6*a*) for ϕ_b. Substituting these results in (2.7), one then solves for ϕ_a directly.

When the coupling is strong, one must resort to the complete coupled equations, (2.4), and integrate them numerically. One procedure, which we shall now develop, reduces the coupled equations to coupled radial linear differential equations by eliminating all the angle and spin dependence. Assume that the potential V^{pt} is a scalar, so that the total angular **J** of the interacting system is conserved. We may therefore restrict the discussion to partial waves with a given J. The angular momentum of the system consists of the spins of the target and projectile j_t and j_p, respectively, added to their relative angular momentum **l**:

$$\mathbf{J} = \mathbf{j}_t + \mathbf{j}_p + \mathbf{l} \tag{2.10}$$

Two coupling schemes that lead to the spin-angle functions with J and M_J quantum numbers have been used. The *channel spin coupling* scheme proceeds in two steps, first coupling the spins,

$$\mathbf{j}_t + \mathbf{j}_p = \mathbf{S} \tag{2.11}$$

and then coupling **S** and **l** to form **J**:

$$\mathbf{S} + \mathbf{l} = \mathbf{J} \tag{2.12}$$

The spin-orbit coupling scheme first couples $\mathbf{j}_p$ and **l** to form $\mathbf{J}_p$ and then couples $\mathbf{J}_p$ to $\mathbf{j}_t$ to form **J**:

$$\begin{aligned} \mathbf{j}_p + \mathbf{l} &= \mathbf{J}_p \\ \mathbf{J}_p + \mathbf{j}_t &= \mathbf{J} \end{aligned} \tag{2.13}$$

The wave functions corresponding to these two coupling schemes are connected by the $6-j$ symbol [see Appendix A, Eq. (2.85), in deShalit and Feshbach (74)]. Which coupling scheme is more convenient to use depends on the physics of the problem: Spin-orbit coupling would be appropriate when the spin-orbit interaction is strong.

We shall provide an explicit discussion of the coupled channel for channel spin coupling only since the algebra is simplest for that case. In order to separate the geometric factors as completely as possible, the dependence on l of $\phi_i(0)$ in (2.1) will be factored out, leaving only the radial dependence. For a given total angular momentum of the system J, z component M, we couple

$$\mathscr{Y}_{lm} = i^l Y_{lm}(\hat{\mathbf{r}}_0)$$

with the channel spin wave function $\psi_\alpha(Sm_s;\mathbf{r})$ to form a wave function with J and M:

$$\Phi_\alpha(JM;S,l) = \sum_{m,m_s} (lmSm_s|JM)\mathscr{Y}_{lm}(\hat{\mathbf{r}}_0)\psi_\alpha(Sm_s;\mathbf{r}) \tag{2.14}$$

The subscript α orders the possible wave functions whose spin is given by J. The variable $\mathbf{r}$ represents all the target nuclear coordinates. The functions Φ_α satisfy

$$\langle \Phi_\alpha(J'M';S,l')|\Phi_\beta(JM;S',l)\rangle = \delta_{JJ'}\delta_{MM'}\delta_{ll'}\delta_{SS'}\delta_{\alpha\beta} \tag{2.15}$$

The integrations are carried out over $\mathbf{r}$, the internal coordinates, and Ω_0, the angular coordinates for the relative motion. The channel spin wave function $\psi(S,m_s)$ is obtained by coupling the target nucleus wave function $\psi(j_t m_t)$ and the spin wavefunction $\chi(j_p m_p)$ of the projectile:

$$\begin{aligned}\psi_\alpha(Sm_s;\mathbf{r}) &= \psi_\alpha((j_p j_t)S(m_s;\mathbf{r}) \\ &= \sum_{m_p,m_t} (j_p m_p j_t m_t|Sm_s)\psi_\alpha(j_t,m_t)\chi(j_p,m_p)\end{aligned} \tag{2.16}$$

One now expands $P\Psi$ in terms of $\Phi_\alpha(JM;Sl)$, in that way providing the dependence of $P\Psi$ on $\mathbf{r}$ and $\hat{\mathbf{r}}_0$. The coefficients of the expansion will then depend only upon r_0. Therefore,

$$P\Psi = \frac{1}{r_0}\sum_{\substack{\alpha \\ JM}} u_\alpha(J(Sl);r_0)\Phi_\alpha(JM;Sl)A(JM;S_i l_i) \tag{2.17}$$

The coefficient $A(JM;S_i l_i)$ is chosen so that the incident channel associated with the ground state of the target and denoted by $S_i l_i$ contains the only incoming wave. We shall determine this coefficient later. Introducing (2.17) yields sets of

coupled differential equations for u_α. Only those u_α with the same J and M will couple. For a given J, these equations are

$$\left\{E-\varepsilon_\alpha+\frac{\hbar^2}{2\mu}\left[\frac{d^2}{dr_0^2}-\frac{l(l+1)}{r_0^2}\right]-(J(Sl)\|V^{(pt)}\|J(Sl))\right\}u_\alpha(J(Sl);r_0)$$
$$=\sum_{\substack{\alpha\neq\alpha'\\ S',l'}}(J(Sl)\|V^{(pt)}\|J(S'l')u_{\alpha'}(J(S'l');r_0) \tag{2.18}$$

The next step is to evaluate the reduced matrix elements of $V^{(pt)}$. For this purpose, we expand $V^{(pt)}$ in a multipole series:

$$V^{(pt)}=\sum \mathbf{Q}_\lambda(\mathbf{r})\cdot\mathbf{Y}_\lambda(\Omega_0)v_\lambda(r_0) \tag{2.19}$$

Note that this expansion assumes a term-by-term factorization of the dependence $\mathbf{r}$ and r_0, which we will justify later. Evaluating the matrix elements can be accomplished by using (A.2.54) of deShalit and Feshbach (74). One obtains

$$(J(Sl)\|V^{(pt)}\|J(S'l')=\sum_\lambda(-)^{l+J+S'}\sqrt{2J+1}\begin{Bmatrix}S & l & J\\ l' & S' & \lambda\end{Bmatrix}$$
$$\times(S\|Q_\lambda\|S')(l\|Y_\lambda\|l')v_\lambda(r_0)$$

Inserting (A.2.48) of deShalit and Feshbach (74) for $(l\|Y_\lambda\|l')$, one finally has

$$(J(Sl)\|V^{(pt)}\|J(S'l'))=\sum_\lambda(-)^{J+S+(l'-l)/2}\sqrt{\frac{(2l+1)(2l'+1)(2\lambda+1)(2J+1)}{4\pi}}$$
$$\times\begin{Bmatrix}S & l & J\\ l' & S' & \lambda\end{Bmatrix}\begin{pmatrix}l & \lambda & l'\\ 0 & 0 & 0\end{pmatrix}(S\|Q_\lambda\|S')v_\lambda(r_0) \tag{2.20}$$

A further reduction is possible since $\mathbf{S}=\mathbf{j}_t+\mathbf{j}_p$, and Q_λ depends only on $\mathbf{r}$. Equation (A.2.55) of deShalit and Feshbach (74) would be used for this purpose. The complete formula is given by Tamura (65). From (2.20) we see that

$$\begin{aligned}&\mathbf{S}+\mathbf{l}=\mathbf{J}\ (a) && \mathbf{l}'+\mathbf{l}=\boldsymbol{\lambda}\ (c)\\ &\mathbf{S}'+\mathbf{l}'=\mathbf{J}\ (b) && \mathbf{S}'+\mathbf{S}=\boldsymbol{\lambda}\ (d)\end{aligned} \tag{2.21}$$

and

$$l+\lambda+l'=\text{even number} \tag{2.22}$$

Equations (2.21a) and (2.21b) express the conservation of angular momentum in the process. Equations (2.21c) and (2.21d) give the changes in l and S induced by the interaction. From (2.22) one obtains the conservation of parity. Note

that in (2.20) the other properties of the target nucleus are contained in the reduced matrix elements $(S \| Q_\lambda \| S')$. In principle, these can be determined from experimental data and compared with the predictions of the theory of the target nucleus.

As long as S' and l' satisfy (2.21*b*), $u(J(S'l'))$ will be coupled to $u(J(Sl))$. The number of coupled equations increases as the number of excited states are included in the calculation. It increases as the energy increases. To illustrate, suppose that the projectile is an α-particle (intrinsic spin 0), so that S equals the angular momentum of the nuclear levels. Suppose these are 0, 2, 4, where the spin of the ground state is 0, and suppose that λ is even. The value of J for the lth particle wave is l. For $S = 2$, $|J - S| < l' < J + S$, so that for $J\,(= l) > S$, l' can be $l-2$, l, or $l+2$. Similarly, for $S = 4$ if $J \geqslant 4$, l' can be $l-4$, $l-2$, l, $l+2$, $l+4$. If $J < 4$, l' can equal $l+4$, $l+2$, l, and as on, breaking off at $l' = 4 - J = 4 - l$. Thus if $J \geqslant 4$, the number of coupled equations is nine. The number of J's is given approximately by $J = l_{\max}$, where $l_{\max} \simeq k_i R$, where k_i is the incident value of k and R is the nuclear radius.

Returning to the coupled equations, (2.18), one particular (S, l) will correspond to incident channel. For that channel

$$u_i(J(Sl)_{r_0 \to \infty} \to e^{-i(k_i r_0 - l\pi/2)} - S_{Ji}(S_i l_i, S_i l_i) e^{i(k_i r_0 - l\pi/2)} \tag{2.23a}$$

For other channels with the same value of J,

$$u_\alpha(J(S'l'))_{r_0 \to \infty} \to - S_{J\alpha}(S_i l_i, S'l') e^{i(k_\alpha r_0 - l'\pi/2)} \tag{2.23b}$$

$S_{J\beta}(Sl; S'l')$ is the S matrix in terms of which the amplitude for elastic and inelastic scattering can be expressed.

Using (2.23) it is now possible to calculate the reaction amplitudes in terms of S_J. One first needs the expansion for the incident wave function, $\Psi^{(i)}_{JM}$, where

$$\begin{aligned}
\Psi^{(i)} &= e^{i\mathbf{k}_i \cdot \mathbf{r}_0} \psi_i(S_i m_{si}; \mathbf{r}) \\
&= 4\pi \sum_{lm} j_l(k_i r_0) Y^*_{lm}(\hat{\mathbf{k}}_i) i^l Y_{lm}(\hat{\mathbf{r}}_0) \psi_i(S_i m_{si}; \mathbf{r}) \\
&= 4\pi \sum_{lm} j_l(k_i r_0) Y^*_{lm}(\hat{\mathbf{k}}_i) \sum_{JM} \Phi(JM; S_i l)(lm S_i m_{si} | JM)
\end{aligned}$$

Therefore,

$$\Psi^{(i)}_{JM} = 4\pi \sum_{lm} j_l(k_i r_0) Y^*_{lm}(\hat{\mathbf{k}}_i) \Phi(JM; S_i l)(lm S_i m_{si} | JM) \tag{2.24}$$

Asymptotically,

$$\Psi^{(i)}_{JM} \to \frac{2\pi i}{k_i r_0} \sum (e^{-i[k_i r_0 - (\pi/2)l]}) - e^{i[k_i r_0 - (\pi/2)l]} Y^*_{lm}(\hat{\mathbf{k}}_i) \Phi(JM; S_i l)(lm S_i m_{si} | JM)$$

Because of the interaction, $\Psi_{JM}^{(i)}$ becomes Ψ_{JM}:

$$\Psi_{JM} \to \frac{2\pi i}{k_i r_0} \sum_{\substack{lm \\ S'l'}} (\delta_{S'S} e^{-i[k(S')-(\pi/2)l]} - S_J(S_i l, S'l') e^{i[k(S')r_0-(\pi/2)l]})$$
$$\times Y_{lm}^*(\hat{\mathbf{k}}_i)\Phi(JM; S'l')(lmS_i m_{si}|JM)$$

Expanding $\Phi(JM; S'l')$ according to (2.14), and taking the z direction to be along $\mathbf{k}_i$ so that

$$Y_{lm}^*(\hat{\mathbf{k}}_i) = \sqrt{\frac{2l+1}{4\pi}}\,\delta_{mo}$$

one finally obtains the reaction amplitude:

$$f_{JM}(S_i, m_{si} \to S', m_s') = \frac{\sqrt{\pi}}{k_i} \sum_{\substack{ll'S' \\ m'm_s'}} i^{l'} \sqrt{2l+1}(l0S_i m_{si}|JM)(l'm'S'm_s'|JM)$$
$$\times [\delta_{S'S_i} - S_J(S_i l, S'l')] Y_{l'm'}(\hat{\mathbf{r}}_0) \tag{2.25}$$

The cross section is given by

$$\sigma(S_i \to S') = \frac{k(S')}{k_i} \frac{1}{2S_i+1} \sum_{m_{si}, m_s'} |f_{JM}(S_i m_{si} \to S' m_s')|^2 \tag{2.26}$$

Although the sums over the m's can be performed analytically, one gains little advantage over inserting (2.25) in (2.26) and summing numerically.

The results obtained for other coupling schemes and the methods used for integrating the differential equations (2.18) are discussed in detail by Satchler (83) in Chapter 5 of his book. With these formalisms, one can discuss inelastic and elastic scattering, including as many possible steps as needed and practicable, extracting from the data the S matrix and finally the target nuclear parameters $(S \| Q_\lambda \| S')$.

For the case of the deformed rotor of Bohr and Mottelson (62), the procedure described above is generally replaced by the adiabatic approximation. In this approximation, the problem is solved, keeping the five macroscopic variables, the three Euler angles giving the orientation of the body-fixed axes with respect to a frame fixed in space, and the two variables β and γ giving the vibrational degrees of freedom about the average deformation β_0 and γ_0. It is assumed that the variation of these five variables during the course of the interaction will be small, a condition that is well satisfied above a rather low projectile energy.

Under these assumptions, we solve for the *elastic* scattering in the *body*-fixed frame, obtaining an amplitude that is a function of β and γ. Transforming to the space-fixed frame, one obtains an amplitude that is a function of β, γ, and

the Eulerian angles. The amplitudes for inelastic or elastic scattering are obtained by taking matrix elements between the initial ground state of the target and the final state.

Let the interaction between the projectile and the target in the body-fixed frame be

$$V_\lambda = \sum_\lambda V_\lambda(r, \alpha, \beta)[i^\lambda Y_{\lambda 0}(\hat{\mathbf{r}}')]^* \tag{2.27}$$

where we have assumed axial symmetry, as indicated by the zero projection of λ along the symmetry axis. Differing orbital angular momenta will be coupled so that the coupled equations for adiabatic elastic scattering take on the form

$$\left[\frac{d^2}{dr^2} + k^2 - \frac{l'(l'+1)}{r^2} - \frac{2m}{\hbar^2}\langle l'\mu|V|l'\mu\rangle\right] u_{l'l}^{(\mu)}(r) = \frac{2m}{\hbar^2}\sum_{l''}\langle l'\mu|V|l''\mu\rangle u_{l''l}^{(\mu)}(r) \tag{2.28}$$

where μ is the projection of $\mathbf{l}$ along the symmetry axis and m is the reduced mass. Note that μ does not change because of the zero projection of $Y_{\lambda 0}$ in the interaction, (2.27). The indicated matrix elements are readily evaluated using (A.2.25) of deShalit and Feshbach (74). One obtains

$$\langle l'\mu|V|l\mu\rangle = \sum_\lambda V_\lambda(r, \alpha, \beta) i^{l-l'-\lambda}(-)^\mu \times \left[\frac{(2l'+1)(2\lambda+1)}{4\pi} 2l+1\right]^{1/2} \begin{pmatrix} l' & \lambda & l \\ \mu & 0 & -\mu \end{pmatrix} \begin{pmatrix} l' & \lambda & l \\ 0 & 0 & 0 \end{pmatrix} \tag{2.29}$$

Using the boundary conditions given in (2.23) suitably modified, one obtains the adiabatic elastic scattering amplitude in the body-fixed frame:

$$f(\mathbf{k}_i \to \mathbf{k}) = \frac{2\pi}{k_i} \sum_{l,l',\mu} [\delta_{l'l} - S_{l'l}^{(\mu)}] Y_{l\mu}^*(\hat{\mathbf{k}}_i) Y_{l'\mu}(\hat{\mathbf{k}}) \tag{2.30}$$

where $\hat{k}$ is taken in the direction of $\mathbf{r}_0$. We now refer $Y_{l\mu}^*$ and $Y_{l'\mu}$ to the space-fixed frame using (A.2.26) of deShalit and Feshbach (74):

$$Y_{l\mu}^*(\hat{\mathbf{k}}_i) Y_{l'\mu}(\hat{\mathbf{k}}) = \sum_{\mu',\mu''} (-)^\mu Y_{l,\mu''} D_{\mu'',-\mu}^{(l)} Y_{l',\mu'} D_{\mu',\mu}^{(l')}$$

The product of the two D functions can be expressed in terms of a single D using (A.2.75) of deShalit and Feshbach (74) with the result

$$Y_{l\mu}^*(\hat{\mathbf{k}}_i) Y_{l'\mu}(\hat{\mathbf{k}}) = \sum_{\mu',\mu'',L} (-)^\mu (2L+1) Y_{l\mu''}(\hat{\mathbf{k}}_i) Y_{l'\mu'}(\hat{\mathbf{k}}) \times \begin{pmatrix} l & l' & L \\ \mu'' & \mu' & M \end{pmatrix} \begin{pmatrix} l & l' & L \\ -\mu & \mu & 0 \end{pmatrix} D_{M0}^{(L)*}$$

But the sums over μ' and μ'' give just the tensor product

$$[Y_l \otimes Y_{l'}]_{L,-M}[(-)^{l-l'+M}/\sqrt{2L+1}],$$

so that

$$f_{L,-M}(k_i \to k) = \frac{2\pi i}{k_i} \sum_{l,l',\mu,L} (-)^{\mu+L} \sqrt{2L+1}[\delta_{l'l} - S_{l'l}^{(\mu)}][Y_l \otimes Y_{l'}]_{L,M} \times \begin{pmatrix} l & L & l' \\ -\mu & 0 & \mu \end{pmatrix} D_{M0}^{(L)} \tag{2.31}$$

The amplitude for a transition from the ground state S_i to an excited state S' is given by $\langle S'|f_{L,-M}(\mathbf{k}_i \to \mathbf{k})|S_i\rangle$. In this context, $f_{L,-M}$ is a tensor of rank L, component M, and will allow the same transitions as an L multipole with the condition $\mathbf{S}' = \mathbf{S}_i + \mathbf{L}$.

From a practical point of view, the usefulness of this approach is limited by the number of coupled differential equations in (2.28). This is determined for a given l by the condition $\mathbf{l}' = \mathbf{l} + \boldsymbol{\lambda}$ and the parity condition $(l + l' + \lambda)$ even. For a small λ, the number of coupled equation will thus be acceptable, although solutions must be obtained for each μ and for all relevant l's.

3. APPLICATIONS

The coupled-channel formalism developed in Section 2 has been applied to elastic and inelastic scattering of a variety of projectiles, nucleons, light and heavy ions, pions by a variety of target nuclei, and over a wide range in energy. Usually, this method of analysis is applied to direct reactions when the DWA approximation or the spherical optical model of Chapter V fails. A *rough* indication of the importance of a given step $(a \to b)$ where an energy-conserving excitation of b is possible is given by the parameter $(1/2\pi)(\mu k_b/\hbar^2)J_{ba}$, where J_{ba} is the volume integral of the coupling potential, k_b the wave number of the projectile after excitation of b, and μ the reduced mass. For example, the strength of a two-step transition $a \to b \to c$ compared to a one-step transition $a \to c$ is given by

$$\frac{1}{2\pi}\frac{\mu k_b}{\hbar^2}\frac{J_{cb}J_{ba}}{J_{ca}}$$

If this quantity is small, it is unlikely that the two-step transition will be of importance. It should be noted that there will always be additional contributions from compound nuclear formation. These can be particularly important at low energies and back angles.

A situation most likely to require the use of the coupled-channel equations occurs when the target nuclear energy levels are collective. In that case, the wave functions of these levels are simply connected, for example, by the application of a raising and lowering operator $\hat{0}$, enhancing the possibility of

relatively strong and coherent coupling between the levels. This will generally take place if a significant component of the projectile–nucleus interaction is proportional to $\hat{0}$. Moreover, because of the simple connection, there will be well-defined phase relations among the various multistep reaction amplitudes, including the single step. Under these circumstances, constructive interference can occur, leading to a strong enhancement of the amplitude; or of course, the interference could be destructive, with a consequent anomalous decrease in cross section. Moreover, the associated angular distributions will, because of the interference, oscillate irregularly.

Not surprisingly, inelastic scattering from deformed and vibrational nuclei furnishes an excellent example of the use of a coupled-channel analysis. The procedure used was proposed by Glendenning Hendrie, and Jarvis (68) for inelastic scattering of 50-MeV α-particles. A spherical optical model potential is adjusted so as to fit the experimental data (angular distribution, total cross section, polarization, etc.) for elastic scattering by spherical nuclei in the neighborhood of the collective target nuclei to be studied and in the projectile energy range of interest. In the case of neutron scattering to be discussed later, this analysis is quite extensive, going to the lowest energies, including the strength functions (Chapter IV), as well as the zero energy scattering length. This potential, (V.2.38), will depend parametrically on radius parameters R_0, R_W, R_D, and R_{s0}, where R_0 enters into the central potential. R_W is the volume absorbing radius, R_D is the surface absorbing radius, and R_{s0} is the spin orbit radius. In most cases the "'standard" form (V.2.38) has been used, the radial dependence given by the Woods–Saxon form, $(1 + e^{(r-R)/a})^{-1}$, and its derivative. To include the effects of deformation, one replaces R (where R can equal R_0, R_W, R_D, or R_{s0}) by (VI.13.1) of deShalit and Feshbach (74):

$$R = R_0(1 + \sum \alpha_{\lambda\mu} Y_{\lambda\mu}(\theta, \phi)) \tag{3.1}$$

for a vibrational nucleus. The coefficients $\alpha_{\lambda\mu}$ are operators. For a deformed nucleus, as we have seen in the preceding section, the calculations are best performed in the body-fixed system, so that one write

$$R = R_0\left(1 + \sum_{\lambda} \beta_\lambda Y_{\lambda 0}(\theta', 0)\right) \tag{3.2}$$

where θ' is the spherical angle in the body-fixed case. The coefficients β_λ are not operators. The next step is to express the resulting potential in the forms given by (2.19) and (2.27). For the case of the vibrating nucleus [see (3.1)], this is accomplished by expanding the potential in a power series in $\sum \alpha_{\lambda\mu} Y_{\lambda\mu}$. The matrix elements of Q_λ [(2.19) and (2.20)] will be proportional to the matrix elements of $\alpha_{\lambda\mu}$ between various vibrational states. For the deformed nucleus according to Tamura (65), the power series in $\sum \beta_\lambda Y_{\lambda 0}$ will not be adequate for large deformations, so that one must collect all the contributions to the coefficient of $Y_{\lambda 0}$ from higher powers of $\sum_\lambda \beta_\lambda Y_{\lambda 0}$.

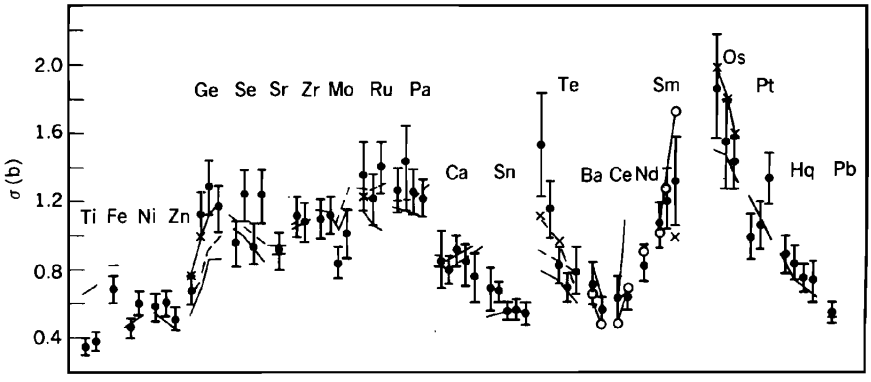

FIG. 3.1. Neutron inelastic scattering cross sections for scattering to first 2^+ levels at incident energies 300 keV above the excitation threshold. [Konobeevskii, Musaelyan, Popov, and Surkova (82)]. [From McEllistrem (85).]

Let us now turn to one example of the use of coupled equations: namely, the study of nuclear reactions induced by neutrons incident on vibrational and deformed target nuclei [McEllistrem (85)]. The strong deformation effects on inelastic neutron scattering are demonstrated by the strong peak in the Sm, Os, and Pt region shown in Fig. 3.1 [Konobeevskii, Musaelyan, Popov, and Surkova (82)]. A similar result is reported by Glasgow and Foster (71), who found that the spherical optical model adjusted to fit the neutron total cross section for a wide range of target nuclei failed for the deformed muclei. Resolution of this difficulty required the coupled-channel analysis of the preceding section. In Fig. 3.2 a comparison is made between the experimental data for neutron scattering by ^{76}Se and ^{80}Se and two models, the spherical vibrator and the deformed potential model, in which the matrix elements are taken from Coulomb excitation. In Fig. 3.3 neutron scattering by ^{194}Pt is compared with the predictions of asymmetric rigid rotor model (ARM) of Davydov and Filippov [see deShalit and Feshbach (74, p. 484)] and the dynamic deformation models (PPQ) of Kumar (69, 85) or the interacting boson model (IBM) model of Arima and Iachello (75, 76, 78, 79) as given for this nucleus by Bijker, Dieprink, Scholten, and Spanhoff (80). A careful treatment of the contribution of the compound nuclear contribution was necessary because of the low neutron energy. In both examples, the central real potential and the surface absorbing potential were deformed. The spin-orbit potential was not deformed. A volume absorbing term was not included. To obtain the most accurate results, it was found necessary to include several of the levels that can couple to the state whose excitation is under study.

In both of these examples we note that one obtains good agreement with the data for both magnitude and angular distributions. Second, it is possible to distinguish among various models. In the case of Fig. 3.2 one can conclude that

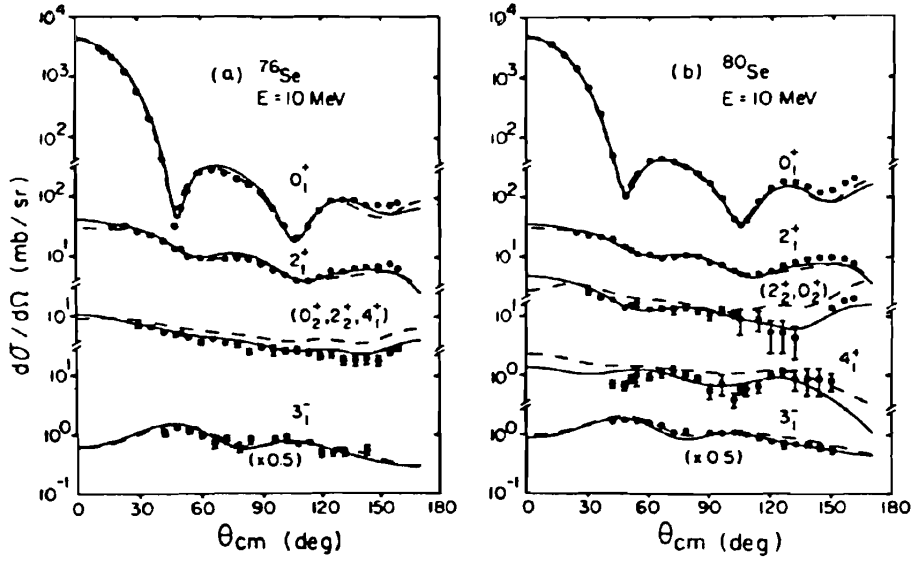

FIG. 3.2. Scattering cross sections for two Se isotopes. Dashed curves are for spherical vibrator calculations. Solid curves result from use of matrix elements deduced from Coulomb excitation measurements. (From McEllistrem (85).]

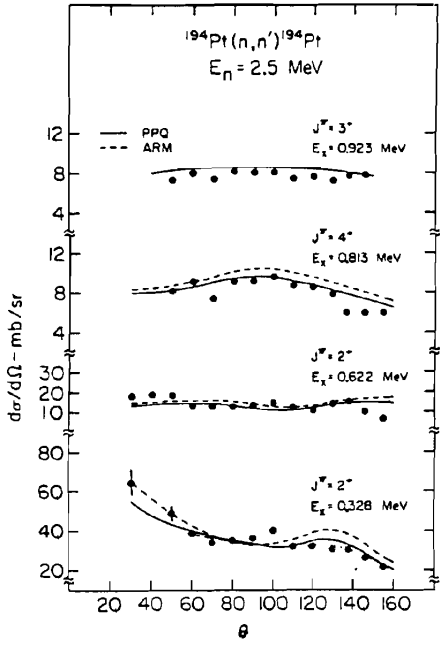

(a)

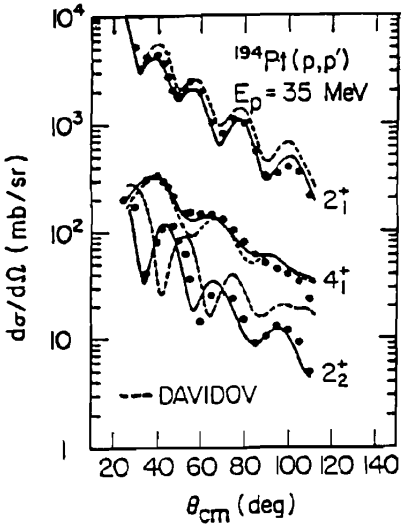

(b)

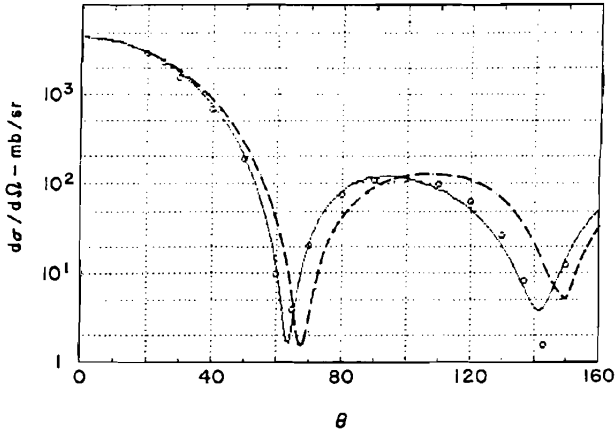

FIG. 3.4. Shape elastic scattering cross sections at 2.5 MeV for neutron scattering by ^{192}Os. Curves are for spherical one-channel (dashed) and for coupled-channel models fitted to the total cross section. [From McEllistrem (85).]

the spherical vibrator model does not describe the Se nuclei. In the Pt case (Fig. 3.3) one sees that the asymmetric rigid-rotor model is inferior to the dynamic deformation or the IBM model. (Note that the ordinates in these figures are the logarithm of the cross section indicated.) The latter models yield a γ soft description of ^{194}Pt for the energy levels, transition probabilities, and inelastic neutron scattering which the *rigid* rotor of the ARM model cannot match. Another conclusion that can be drawn from Fig. 3.2 and other investigations is that within a few percent the quadrupole moment for the *charge* distribution and for the *matter* distribution are equal. More generally, values of the deformation parameters β_λ obtained from neutron scattering are in agreement with values obtained with other probes.

The effects of deformation are also visible in the elastic scattering. Both the spherical potential and the coupled-channel potentials are adjusted so as to yield good agreement with the total cross section for neutrons, with energies between 0.25 and 4 MeV incident on ^{192}Os. The angular distributions calculated with these two options are substantially different (see Fig. 3.4)—with agreement with the data being obtained with the coupled-channel analysis.

FIG. 3.3. (*a*) Measured and calculated inelastic cross sections for the first four excited levels. PPQ is the model of Kumar (69). ARM is the asymmetric rotator model of Davydov and Filippov (58). (*b*) Inelastic scattering cross sections for lowest three excited levels. The solid curves are for the IBA model. [From MeEllistrem (85).]

4. COUPLED-CHANNEL BORN APPROXIMATION (CCBA) AND TRANSFER REACTIONS

The examples of Section 3 demonstrate the strong coupling that a band of collective states exhibits in elastic and inelastic scattering, requiring the use of coupled channels. In a transfer reaction, one must take that coupling into account, as the transition between the target nucleus and the residual nucleus may be preceded by inelastic scattering to various members of the target nucleus band, and/or may be followed by inelastic scattering to members of residual nucleus collective band states.

The DWA was based on a two-channel *ansatz* for stripping given by (VI.2.3):

$$P\Psi = \mathscr{A}[u\phi + v\chi\psi] \tag{VI.2.3}$$

In this equation, ϕ is the wave function of the residual nucleus, χ the internal deuteron wave function, ψ the ground-state wave function of the target nucleus, and u and v the channel wave functions for the proton and deuteron, respectively. The resultant DWA matrix element is given by (VI.2.46′):

$$\mathscr{T}_{dp}^{(\mathrm{DWA})} = \langle U_{0,f}^{(-)}\phi | \mathscr{V}^{(f)} \mathscr{A}(v_{0,i}^{(+)}\chi\psi)\rangle \tag{VI.2.46′}$$

where $v_{0,i}$ is usually taken to be the deuteron optical single-channel wave function. (For the definition of the other-symbols, see Section VI.2.) To take the excited states of the target nucleus into account (we shall deal with this case only; the reader should be able to discuss the effect of including the excited states of the residual nucleus), one replaces (VI.2.3) as follows:

$$P\Psi = \mathscr{A}[u\phi + (\textstyle\sum v_\alpha\psi_\alpha)\chi] \tag{4.1}$$

The wave functions for the states of the target nucleus are given by ψ_α. The corresponding deuteron–nucleus channel wave functions are given by v_α. The analysis given in Section VI.2 beginning with (VI.2.3) is readily generalized. The major change is in the K matrix, which instead of being a 2×2 matrix is now an $(n+1) \times (n+1)$ matrix, where n equals the number of states of the target nucleus included in the sum in (4.1). The equations of Section VI.2 can be taken over completely if one replaces the v and V of that section by a semicolumnar matrix with elements v_α and V_α. The DWA approximation, now renamed CCBA, is obtained by neglecting the overlap integrals and the coupling to the proton channel. The result, replacing (VI.2.46′), is

$$\mathscr{T}_{dp}^{(\mathrm{CCBA})} = \sum_\alpha \langle U_{0,f}^{(-)}\phi | \mathscr{V}^{(f)} \mathscr{A}(v_{0,\alpha}^{(i)}\psi_\alpha\chi)\rangle \tag{4.2}$$

where $v_{0,\alpha}^{(i)}$ are solutions of the many-channel optical model Schrödinger equation describing elastic and inelastic scattering of the deuteron by the target nucleus.

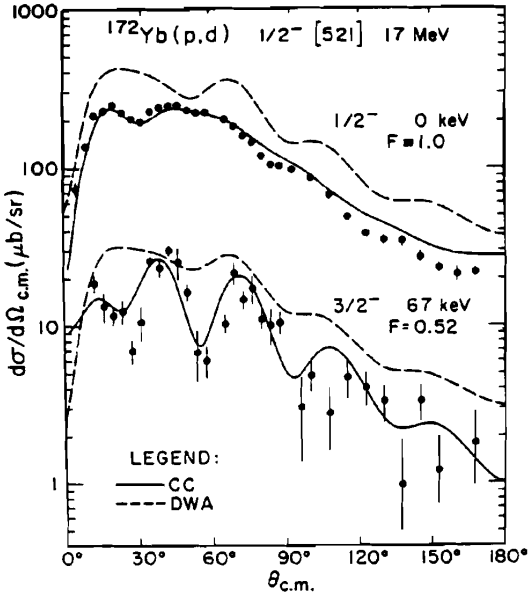

FIG. 4.1. Data and calculations for ^{172}Yb$(p,d)^{171}$Yb leading to the first two members of the ground band. The cross-section scale is the experimental one. The probable error for the absolute cross-section normalization is $\sim 30\%$. The coupled-channel calculations have been normalized individually for each state to the data. [From Ascuitto, King, McVay, and Sørensen (74).]

These are just the coupled-channel equations of Section 2 of this chapter. A particular procedure for determining the reaction amplitude, known as the *source term method* has been developed by Ascuitto and Glendenning (69). For a review, see Ascuitto and Seglie (84).

As may be expected, it is important to use the CCBA when the nuclei involved are deformed or vibrational. An example is given in Fig. 4.1, in which the DWA and CCBA predictions for pickup reaction ^{172}Yb(p, d) are compared with each other and with experiment. The improvement obtained using the CCBA is striking.

The analysis sketched above, taking the effect of inelastic channels into account, can readily be extended to include a more general set of channels. The K matrix can be generalized as that the resulting coupled-channel equations would then take both antisymmetry and overlap into account. Neglecting the latter will then yield a CCBA approximation in the form given by (4.2). The nontrivial problem that remains is one of physics. What are the important channels? Or stated in terms of the multistep concept, what are the important intermediate states that need to be taken to account?

5. STATISTICAL DIRECT AND COMPOUND MULTISTEP REACTIONS[†]

When the number of possible intermediate states becomes large, the solution of the resulting couple-channel equations becomes impractical and uninformative. If the intermediate states do not have the strong interconnections, exhibited for example by the collective states, the detailed analysis provided by coupled-channel equations should be unnecessary. Under each or both of these circumstances, a method that will provide reasonably accurate predictions of the gross (macro) structure of the experimental cross section but will not be able to reproduce the finer details, the microstructure, is suggested. The development of such a formalism is the main subject of this section. A statistical method similar to one used in Section IV.7 will be employed. It will yield expressions for the average cross sections. Such an analysis will necessarily omit the cross sections arising out of special circumstances, such as those associated with isolated doorway states. In most cases these are to be added to the statistical ones we shall be concerned with now.[‡]

In this theory, the number of steps can be as large as is necessary. Under these circumstances, the genesis of the formation of the compound nucleus will be developed automatically. The theory provides a step-by-step description of this process and will thus include the possibility that it may be interrupted before the compound state is achieved, leading to the statistical multistep compound reaction.

We begin by recalling the discussion in the introduction to this chapter, where it was shown that the various reaction types are closely correlated with the interaction time, which in turn is roughly measured by the number of steps involved. The greater the number of steps, the greater the complexity of the wave functions. The wave function associated with the single-step direct reaction is the simplest and that describing the compound nucleus is the most complex. The multistep direct reaction may involve several steps. The multistep compound reaction will also involve several steps. For each of these, the process may be terminated by emission to the final state. The flux that survives goes on to form the compound nucleus. Thus the wave function for the multistep compound reaction has components from the steps leading to the compound nucleus plus the compound nuclear component.

This discussion suggests that it would be advantageous to classify the states of the system in increasing order of complexity. An example employing the shell model is illustrated in Fig. 5.1. The incident channel consists of a nuclear projectile and a target nucleus represented schematically by nucleons in a potential well. As a result of the interaction between the incident nucleon and the target nucleus, one of the nucleons in the nucleus will gain energy while the projectile will lose energy. Two situations can occur: one set of states, in which none of the nucleons are in the continuum, is labeled Q space, and another

[†]Feshbach, Kerman, and Koonin (80); Feshbach (73); Bonetti, Chadwick, Hodgson, Carlson and Hussein (91).

[‡]See, however, Bonetti et al. (91) Sec. 6.

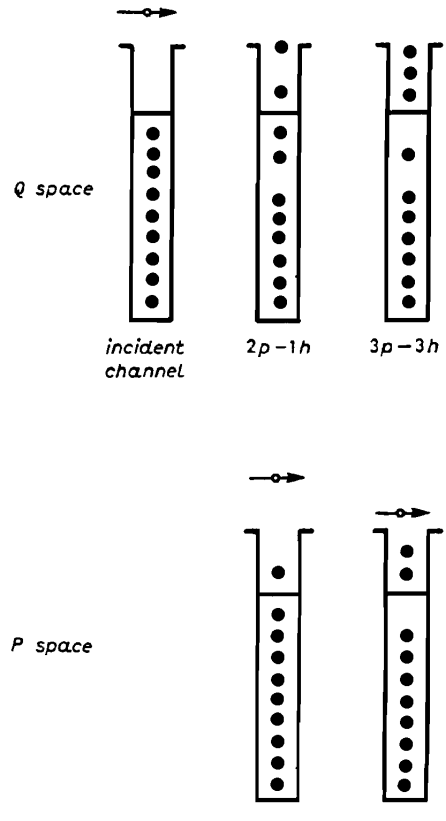

FIG. 5.1. Schematic shell model example of increasing complexity.

set, in which at least one nucleon is in the continuum is labeled P space. In Q space the interaction results in the formation of a two-particle/one-hole ($2p$–1h) state. Further interactions can result in 3p–2h states; 4p–3h states, and so on. These (the 1p, 2p–1h, 3p–2h, etc.) are a series of states of increasing complexity. In the case of the P space, the target nucleus, on interacting with the projectile, can be excited to a 1p–1h state, and on further interactions with the projectile, be excited to a 1p–1h state, a 2p–2h state, and so on, again a series of states of increasing complexity.

More generally, the Hilbert space of the problem can be broken up into orthogonal subspaces, each of which contains all the states of a given complexity. This partition is illustrated in Fig. 5.2. In terms of the example, the "box" P_0 contains the incident nucleon plus the unexcited target nucleus. The P_1 box contains all the 1p–1h excitations and one nucleon in the continuum. The P_2 box contains all the 2p–2h excitations, and so on. On the other hand, the Q_1 box contains all the 2p–1h excitations, the Q_2 the 3p–2h excitations, and so on. The chain ends at Q_r. The rth stage is defined to be the one at which the

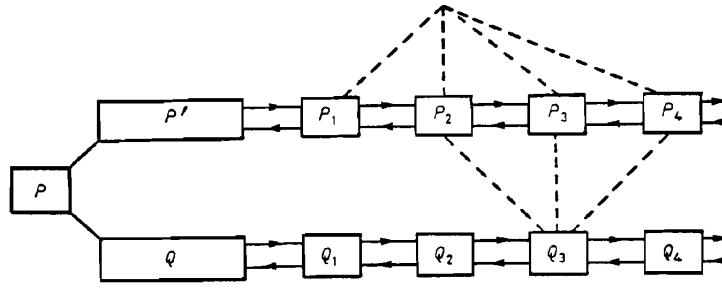

FIG. 5.2. Partition of Hilbert space into subspace of increasing complexity indicated by the subscript.

system is "trapped" as described in the introduction to Section 5; that is, the ratio of probability of emission compared to the probability of developing more complex configurations is small. This component of the wave function therefore, lives, a relatively long time and "equilibrium" is established. It should be referred to as the compound nuclear component, while *precompound* or *preequilibrium* refers to the preceding $(r-1)$ stages. At low energies, one may expect that r will be small; that is, the compound nucleus is established after just a few interactions.

To progress further, two principal assumptions are made. The first is the *chaining hypothesis.* It assumes that the interaction can change the complexity of the wave function by at most one unit. Thus the interaction can move the system from box P_3 to boxes P_4 and P_2 but not to one labeled P_5. An identical condition holds for the boxes Q_n and for transitions from Q space to P' space.

One can distinguish two differing processes corresponding to the two chains, P' and Q. In one, referred to as the *statistical multistep compound reaction*, the system is confined to the Q-space chain. A transition to the final state can occur at any stage along the chain in Q space by a transition to P space as indicated in Fig. 5.2 and then to the final state. Because of the chaining hypothesis, three stages in P space, P_n, $P_{n\pm1}$, will be involved as the emission from a given stage. The final wave function is composed of contributions from all stages, as indicated in Fig. 5.2. At each stage there is a probability that the reaction terminates and a probability that it continues on to the next stage. When the latter probability is unity, complete equilibrium will develop and the compound nuclear evaporation process will dominate. The chaining hypothesis is exact if the residual interaction acting in each chain is composed of two-body potentials. Note that the chaining hypothesis is the generalization of the doorway state hypothesis of Chapter III. That hypothesis asserted that there was a state or states through which the system had to pass before the compound nucleus is formed. As can be seen from Fig. 5.2, such states are contained in subspace Q. But now wave functions in subspace Q_2 act as doorways for the rest of the

chain. A statistical theory involving the primary doorways, those in Q_1, is, in retrospect, contained in the paper by Block and Feshbach (63).

The second process, indicated in Fig. 5.2, is one in which the system is confined to P' space and is referred to as the *statistical multistep direct process.* The equations describing that reaction type are just the coupled equations, all of them, which was the main subject of the preceding sections of this chapter.

The second principal assumption is the random phase approximation. This was discussed in Section IV.7. The principal result is as follows: Let

$$u = \sum_n u_n \tag{5.1}$$

Moreover, let the phase average [see Section IV.7, the equation below (IV.7.2)] of u and u_n be zero:

$$\langle u \rangle = 0 \qquad \langle u_n \rangle = 0 \tag{5.2}$$

(If these conditions are not satisfied, consider $u - \langle u \rangle$ and $u_n - \langle u_n \rangle$). Then the random phase approximation yields

$$\langle |u|^2 \rangle = \sum_n |u_n|^2 \tag{5.3}$$

In applying the random phase approximation, one assumes that the phases of the components, u_n, are random, and that each value of the phase occurs with equal probability. Therefore, the phase-averaged values yield the expectation value of u and $|u|^2$. We recall the physics underlying the random phase hypothesis. It is that the wave functions are so complex that the matrix elements of the short-range interaction involving them are to a good approximation random variables. The consequence, according to (5.3), is the absence of any interference terms.

This is, of course, not the case when the states involved are members of a collective band, a situation we described earlier in this chapter. In that event, for example, when the nuclei are deformed, one must expand the P subspace of Fig. 5.2 to include the solutions of the coupled equations as described in Section 2. The initial wave function for subspace P is then given by (2.17) or the adiabatic "elastic" wave function involving the $u_{ll}^{(\mu)}(r)$ in (2.28).

The random-phase approximation has an immediate consequence for the Q chain. Since all the states involved are bound, the appropriate quantum numbers are angular momentum and parity. The sum over n becomes a sum over these quantum numbers. Equation (5.3) tells us that terms with differing parity do not interfere. If the u_n are transition matrix elements, $|u|^2$ will be proportional to the differential cross section and one can immediately draw the conclusion that the angular distribution for the statistical multistep compound reaction will be symmetric around 90°, an important result. [For a more detailed discussion, see the discussion following (IV.7.9).]

In the case of the statistical multistep direct reaction, the quantum numbers involved include not only by the angular momentum and parity of the residual nucleus but also the momentum **k** of the system in the continuum state. The angular distribution is, as we shall see, quite similar to that of the single-step direct reaction, that is, peaked in the forward hemisphere. It will differ from the single-step angular distribution in not decreasing as rapidly as the single step as the backward hemisphere is approached. The substantially different behavior of the Q-chain and P-chain wave functions requires partitioning of the Hilbert space into the Q and P sectors.

A. Statistical Multistep Direct Reactions

We begin with

$$(E - H_{\text{eff}})P\Psi = 0 \tag{1.2}$$

where H_{eff} is the multichannel optical model Hamiltonian. This equation was the starting point for the coupled-channel analysis discussed in Section 2. As in that case, one decomposes H_{eff} with a diagonal part, $H^{(D)}$, and a coupling interaction v with respect to an appropriate set of wave functions:

$$H_{\text{eff}} = H^{(D)} + v \tag{5.4}$$

In the example of inelastic scattering discussed in Section 2, that set is made up of the wave functions ψ_α for the states of the target nucleus, so that

$$\begin{aligned} H^{(D)} &= \sum_\alpha \psi_\alpha \rangle \langle \psi_\alpha | H_{\text{eff}} \psi_\alpha \rangle \langle \psi_\alpha \equiv \sum_\alpha \psi_\alpha \rangle H_\alpha \langle \psi_\alpha \\ v &= \sum_{\alpha \neq \beta} \psi_\alpha \rangle \langle \psi_\alpha | H_{\text{eff}} \psi_\beta \rangle \langle \psi_\beta \end{aligned} \tag{5.5}$$

In terms of $H^{(D)}$ and v, (1.2) can be rewritten as follows:

$$P\Psi_i^{(+)} = \phi_i^{(+)} + \frac{1}{E^{(+)} - H_{\text{eff}}} v\phi_i^{(+)} \tag{5.6}$$

where $\phi_i^{(+)}$ the incident wave satisfies

$$(E - H^{(D)})\phi_i = 0 \tag{5.7}$$

The $\mathcal{T}$ matrix for transitions induced by v following from (5.6) is

$$\mathcal{T}_{fi} \equiv \langle \phi_f^{(-)} v P \Psi_i^{(+)} \rangle = v_{fi} + \left\langle \phi_f^{(-)} v \frac{1}{E^{(+)} - H_{\text{eff}}} v\phi_i^{(+)} \right\rangle \tag{5.8}$$

where $\phi_f^{(-)}$ is a solution of (5.7) describing the final state and v_{fi} is defined by

$$v_{fi} \equiv \langle \phi_f^{(-)} v \phi_i^{(+)} \rangle \tag{5.9}$$

The first term in (5.8) is the single-step amplitude. The multistep (more than one) is given by the second term. We shall refer to it as $\mathcal{T}_{fi}^{(\mathrm{msd})}$, where (msd) symbolizes multistep direct. Explicitly,

$$\mathcal{T}_{fi}^{(\mathrm{msd})} = \sum_{\mu} \mathcal{T}_{fi}^{(\mu)} \tag{5.10}$$

where

$$\mathcal{T}_{fi}^{(\mu)} = \left\langle \phi_f^{(-)} P_f v_{f\mu} P_\mu \frac{1}{E^{(+)} - H_{\mathrm{eff}}} P_1 v_{1i} P_i \phi_i^{(+)} \right\rangle \tag{5.11}$$

In this equation P_μ is a projection operator that projects onto the subspace P_μ of Fig. 5.2. These operators satisfy the orthogonality condition,

$$P_\mu P_\nu = P_\mu \delta_{\mu\nu} \tag{5.12}$$

In terms of these operators

$$v = \sum v_{\mu\lambda} \qquad v_{\mu\lambda} = P_\mu v P_\lambda \tag{5.13}$$

Equation (5.11) makes use of this expansion as well as the chaining hypothesis,‡ which asserts that the interaction takes the system from its initial state to the subspace P_1. The amplitude $\mathcal{T}_{fi}^{(\mu)}$ describes passage of the system from the initial state to the first-stage subspace projected by P_1, followed by propagation until the μth stage is reached. At this point the transition to the final state occurs.

The chaining hypothesis is now employed to factorize $P_\nu (E^{(+)} - H_{\mathrm{eff}})^{-1} P_1$. In the appendix to this chapter it is shown that

$$P_\mu \frac{1}{E^{(+)} - H_{\mathrm{eff}}} P_1 = G_\mu v_{\mu,\mu-1} P_{\nu-1} \frac{1}{E^{(+)} - H_{\mathrm{eff}}} P_1 \tag{5.14}$$

Hence

$$P_\mu \frac{1}{E^{(+)} - H_{\mathrm{eff}}} P_1 = G_\mu v_{\mu,\mu-1} G_{\mu-1} v_{\mu-1,\mu-2} \cdots G_2 v_{21} G_1 \tag{5.15}$$

‡There is no implied limitation since one can always define the subspace P_1 as containing those wave functions generated from ϕ_ν by the action of v and orthogonalized with respect to v [see Feshbach, Kerman, and Koonin (80)].

In these equations G_μ satisfies the recurrence relation

$$G_\mu = \frac{1}{E - H_\mu^{(D)} - v_{\mu,\mu+1} G_{\mu+1} v_{\mu+1,\mu}} \tag{5.16}$$

and

$$G_M = \frac{1}{E - H_M^{(D)}} \tag{5.17}$$

M is chosen to be so large ($M \to \infty$) that G_{M+1} can be taken to be zero. This corresponds to the cutoff used in the coupled-channels analysis of Section 2 to obtain a finite number of equations. Here, however, no limit is placed on M.

Inserting (5.15) into the expression (5.11) for $\mathcal{T}_{fi}^{(\mu)}$ yields

$$\mathcal{T}_{fi}^{(\mu)} = \langle \phi_f^{(-)} v_{f\mu} G_\mu v_{\mu,\mu-1} G_{\mu-1} v_{\mu-1,\mu-2} \cdots v_{2,1} G_1 v_{1i} \phi_i^{(+)} \rangle \tag{5.18}$$

Thus the system enters subspace P_1 via the interaction v_{1i}, propagates in this space according to G_1, makes a transition to subspace P_2, and so on, eventually arriving at the P_μ subspace and after propagation in that space makes a transition to the final state.

The multistep cross section is proportional to

$$\sum_{\mu\nu} \mathcal{T}_{fi}^{(\mu)*} \mathcal{T}_{fi}^{(\nu)}$$

In virtue of the random-phase hypothesis, only the $\mu = \nu$ terms survive. Hence

$$\begin{aligned} \left\langle \sum \mathcal{T}_{fi}^{(\mu)*} \mathcal{T}_{fi}^{(\nu)} \right\rangle &= \sum \mathcal{T}_{fi}^{(\mu)*} \mathcal{T}_{fi}^{\mu} \\ &= \sum_\mu \langle \phi_f^{(-)} | v_{f\mu} G_\mu v_{\mu,\mu-1} \cdots v_{21} G_1 v_{1i} v_{i1}^* G_1^* v_{12}^* \cdots v_{\mu-1,\mu}^* G_\mu^* v_{\mu f}^* | \phi_f^{(-)} \rangle \end{aligned} \tag{5.19}$$

To proceed further, we make a spectral decomposition of G_μ using the eigenfunctions of G_μ^{-1} defined by

$$(H_\mu^{(D)} + v_{\mu,\mu+1} G_{\mu+1} v_{\mu+1,\mu}) \psi_{\mu,\alpha} = \left(\varepsilon_{\mu\alpha} + \frac{\hbar^2}{2m} k_\mu^2 \right) \psi_{\mu,\alpha} \tag{5.20}$$

where $\varepsilon_{\mu\alpha}$ and $\hbar^2/2mk_\mu^2$ are the energies of the residual nucleus and the particle in the continuum, respectively. Then

$$G_\sigma = \sum_\alpha \int \frac{d\mathbf{k}_\sigma}{(2\pi)^3} \frac{\psi_{\sigma\alpha}^{(+)} \rangle \langle \tilde{\psi}_{\sigma\alpha}^{(+)}}{E^{(+)} - (\hbar^2/2m) k_\sigma^2 - \varepsilon_{\sigma\alpha}} \tag{5.21}$$

where[‡]

$$\langle \tilde{\psi}^{(+)}_{\alpha,\beta}, \psi^{(+)}_{\sigma\alpha} \rangle = \delta_{\alpha\beta}$$

As Austern and Vincent (74) pointed out, the terms in this expansion will fluctuate strongly. Their phase must be carefully taken into account to obtain a correct result. Since G_σ is well behaved, there must be considerable interference, resulting in substantial cancellations. The use of the random phase approximation under such circumstances would therefore lead to serious errors. Resolution of this difficulty [Feshbach (85, 86)] exploits the fact that G_σ is well behaved. Therefore, one can energy-average G_σ without affecting its value appreciably. The result of the averaging yields the following replacements:

$$\tilde{\psi}^{(+)}_{\sigma\alpha} \to \chi^{(-)}_{\sigma\alpha} \qquad \psi^{(+)}_{\sigma\alpha} \to \chi^{(+)}_{\sigma\alpha} \tag{5.22}$$

to be made *within the interaction region.* The functions $\chi^{(\pm)}$ are eigenfunctions of a new Hamiltonian $\bar{H}_{\text{eff}}$. The change from H_{eff} is a consequence of the energy average. This energy is noted at this point because it emphasizes the character of G_σ. However, it should be noted than an energy average is required in any event by the developments that follow.

We now substitute (5.21) into (5.19), making the replacements given by (5.22) in the matrix elements. To illustrate the resulting calculation, consider the terms in (5.19), which deal with G_1 and couples to states in P_2:

$$\begin{aligned} v_{21} G_1 v_{1i} v^*_{i1} G^*_1 v^*_{12} = \int \frac{d\mathbf{k}_1}{(2\pi)^3} \int \frac{d\mathbf{k}'_1}{(2\pi)^3} \sum_{\alpha,\beta} \bar{v}_{\gamma\alpha}(\mathbf{k}_2, \mathbf{k}_1) \\ \times \frac{1}{E - (\hbar^2/2m)k_1^2 - \varepsilon_{1\alpha} + i\eta} \bar{v}_{\alpha i}(\mathbf{k}_1, \mathbf{k}_i) \\ \times \bar{v}^*_{i\beta}(\mathbf{k}_i, \mathbf{k}'_1) \frac{1}{E - (\hbar^2/2m)k'^2_1 - \varepsilon_{1\beta} - i\eta} \bar{v}^*_{\beta\gamma'}(\mathbf{k}'_1, \mathbf{k}'_2) \end{aligned} \tag{5.23}$$

where

$$\bar{v}_{\gamma\alpha}(\mathbf{k}_2, \mathbf{k}_1) \equiv \langle \chi^{(-)}_{2\gamma}(\mathbf{k}_2) | v \chi^{(+)}_{1\alpha}(\mathbf{k}_1) \rangle \tag{5.24}$$

One now makes use of the random phase approximation, which asserts that

[‡]Let $H_{\text{eff}} = H_0 + v$. Let $\phi_{0\alpha}$ be an eigenfunction of H_0. Then

$$\psi^{(+)}_{\sigma\alpha} = \phi_{\sigma\alpha} + \frac{1}{E^{(+)} - H_{\text{eff}}} V \phi_{\sigma\alpha}$$

and

$$\tilde{\psi}^{(+)}_{\sigma\alpha} = \phi_{\sigma\alpha} + \frac{1}{E^{(+)} - H^\dagger_{\text{eff}}} V^\dagger \phi_{\sigma\alpha}$$

the only surviving contribution to the sum over α and β comes from the $\alpha = \beta$ terms. We note again that this assumes that the matrix elements of v appearing in (5.23) and (5.19) are random variables with an average value of zero. The resulting sum over α involves an energy integral over $\varepsilon_{1\alpha}$. This integral can be done presuming that the major contributions come from the singularities in the propagators. Then one may replace the matrix elements in (5.23) by energy averages taken in the neighborhood of the singularity. The integral over $\varepsilon_{1\alpha}$ becomes

$$I = \int \frac{M(\varepsilon_{1\alpha}, \mathbf{k}_1, \mathbf{k}'_1)}{[E - (\hbar^2/2m)k_1^2 - \varepsilon_{1\alpha} + i\eta][E - (\hbar^2/2m)k_1'^2 - \varepsilon_{1\alpha} - i\eta]} \rho_1(\varepsilon_{1\alpha})\, d\varepsilon_{1\alpha}$$

where ρ_1 is the density of states, χ_α. M is a product of the matrix elements $\bar{v}_{\gamma\alpha}\bar{v}_{\alpha i}\bar{v}^*_{i\alpha}\bar{v}^*_{\alpha\gamma}$, which we replace by a constant with respect to $\varepsilon_{1\alpha}$, obtained by suitably energy averaging about the singularities in the denominator. One then obtains

$$I \simeq \rho_1\left(E - \frac{\hbar^2}{2m}k_1^2\right) M\left(E - \frac{\hbar^2}{2m}k_1^2, \mathbf{k}_1, \mathbf{k}'_1\right) \frac{2\pi i}{(\hbar^2/2m)(k_1^2 - k_1'^2) + 2i\eta} \tag{5.25}$$

The last factor can be written as the sum of a principal values and δ-function. Equation (5.25) is now inserted into (5.23) and the integration over $\mathbf{k}_1$ and $\mathbf{k}'_1$ performed. Assuming a slow variation of M with respect to k'_1 near k_1, the principal-value part of the integral over k'_1 vanishes. When k'_1 differs appreciably from k_1, the integrand is zero as a consequence of the random phase approximation as applied to the sum over α. Hence

$$I \simeq \frac{4\pi m}{\hbar^2}\rho_1\left(E - \frac{\hbar^2}{2m}k_1^2\right) M\left(E - \frac{\hbar^2}{2m}k_1^2, \mathbf{k}_1, \mathbf{k}'_1\right)\delta(k_1^2 - k_1'^2)$$

Thus

$$v_{21}G_1 v^*_{i1}G^*_1 v^*_{12} = \int \frac{d\mathbf{k}_1}{(2\pi)^3}\int \frac{d\mathbf{\Omega}'_1}{4\pi}\frac{mk_1}{\hbar^2}\rho_1(U_1)\sum_\alpha{}' \bar{v}_{\gamma\alpha}(\mathbf{k}_2, \mathbf{k}_1)\bar{v}_{\alpha i}(\mathbf{k}_1, \mathbf{k}_i)$$
$$\times \bar{v}^*_{i\alpha}(\mathbf{k}_i, k_1\mathbf{\Omega}'_1)\bar{v}^*_{\alpha\gamma'}(k_1\mathbf{\Omega}'_1, \mathbf{k}'_2) \tag{5.26}$$

where

$$U_1 = E - \frac{\hbar^2}{2m}k_1^2 \tag{5.27}$$

and the prime on the sum over α indicates that only those configurations in the subspace P_1 whose energy equals U_1 are to be included in the sum. The final step is to apply the random phase approximation to the sum:

$$\sum_{\alpha}^{\prime} \bar{v}_{\gamma\alpha}(\mathbf{k}_2, \mathbf{k}_1)\bar{v}_{\alpha i}(\mathbf{k}_1, \mathbf{k}_i)v^*_{i\alpha}(\mathbf{k}_i, k_1\boldsymbol{\Omega}'_1)v_{\alpha\gamma'}(k_1\boldsymbol{\Omega}'_1, \mathbf{k}'_2)$$

$$= \delta(\boldsymbol{\Omega}_1 - \boldsymbol{\Omega}'_1)\langle \bar{v}_{\gamma 1}(\mathbf{k}_2, \mathbf{k}_1)|\bar{v}_{1i}(\mathbf{k}_1, \mathbf{k}_2)|^2 \bar{v}^*_{1\gamma}(\mathbf{k}_1, \mathbf{k}'_2)\rangle \tag{5.28}$$

The bracketed expression is defined by this equation. The replacement of α by the numerical subscript serves to indicate that an average of the matrix element over the states in subspace P_1 must be taken.

Substituting (5.28) into (5.26) yields

$$v_{21}G_1 v_{1i}v^*_{i1}G^*_1 v^*_{12} = \int \frac{d\mathbf{k}_1}{(2\pi)^3}\frac{mk_1}{4\pi\hbar^2}\rho_1(U_1)\langle \bar{v}_{\gamma 1}(\mathbf{k}_2, \mathbf{k}_1)|\bar{v}_{1i}(\mathbf{k}_1, \mathbf{k}_i)|^2 \bar{v}_{1\gamma'}(\mathbf{k}_1, \mathbf{k}'_2)\rangle$$

This result can be substituted in (5.19) and the analysis repeated with respect to the variables γ, γ', k'_2, and so on, until one comes to the μth contribution, which connects to the final state.

There is still one more averaging to be performed. The final state $\phi_f^{(-)}$ is a linear combination of contributions from each subspace. Experimentally, it is not generally possible to isolate a particular final state; rather, the energy average is measured. We must therefore take an energy average of the results obtained from (5.19), that is, over $\phi_f^{(-)}$. If one again assumes that the contribution from each subspace is random, and therefore employs the random phase approximation, the cross section becomes an incoherent sum of contributions from the subspaces connected to the μth by the interaction v. Because of the chaining hypothesis, this will include contributions from $P_{\mu+1}$ and $P_{\mu-1}$. The average multistep differential cross section following from (5.19) can now be obtained. *The single-step cross section must be added* to the multistep contribution to obtain the complete answer.

The multistep contribution denoted by the subscript msd is

$$\left[\frac{d^2\sigma(\mathbf{k}_f, \mathbf{k}_i)}{d\Omega_f\, dU_f}\right]_{\text{msd}} = \sum_{\substack{m=\mu\pm 1 \\ \mu}} \int \frac{d\mathbf{k}_1}{(2\pi)^3}\cdots\int \frac{d\mathbf{k}_\mu}{(2\pi)^3}\left[\frac{d^2 w_{m,\mu}(\mathbf{k}_f, \mathbf{k}_\mu)}{d\Omega_f\, dU_f}\right]$$

$$\times\left[\frac{d^2 w_{\mu,\mu-1}(\mathbf{k}_\mu, \mathbf{k}_{\mu-1})}{d\Omega_\mu\, dU_\mu}\right]\cdots\left[\frac{d^2 w_{2,1}(\mathbf{k}_2, \mathbf{k}_1)}{d\Omega_2\, dU_2}\right]\left[\frac{d^2\sigma_{1i}(\mathbf{k}_1, \mathbf{k}_i)}{d\Omega_1\, dU_1}\right] \tag{5.29}$$

where

$$\frac{d^2 w_{\nu,\nu-1}(\mathbf{k}_\nu, \mathbf{k}_{\nu-1})}{dU_\nu\, d\Omega_\nu} = 2\pi^2\rho(k_\nu)\rho_\nu(U_\nu)|\bar{v}(\mathbf{k}_\nu, \mathbf{k}_{\nu-1})|^2_{\text{av}} \tag{5.30}$$

measures the probability that the system passes from the $(\nu-1)$st stage to the

νth with the continuum particle momentum changing from $\mathbf{k}_{\nu-1}$ to $\mathbf{k}_\nu$. The density of states of the continuum particle and the residual nucleus are given by $\rho(k_\nu)$ and $\rho_\nu(U_\nu)$, respectively, where

$$E = U_\nu + \frac{\hbar^2}{2m} k_\nu^2 \tag{5.31}$$

Finally, $d\sigma_{1i}/d\Omega_1\, dU_1$ is the average cross section for forming the first stage. It is given by

$$\frac{d\sigma_{1i}}{dU_1\, d\Omega_1} = \frac{2\pi m}{\hbar^2 k_i} \rho(k_1)\rho_1(U_1)|\bar{v}_{1i}(\mathbf{k}_1, \mathbf{k}_i)|^2_{\text{av}} \tag{5.32}$$

Note that in these formulas the distorted wave for the continuum particle has been normalized to a plane wave of unit amplitude at infinity.

The statistical multistep direct cross section, (5.29), for μ steps is expressed as a convolution of the probabilities for each step to occur. Quantum mechanics enters only in the calculation of these probabilities, which involves a DWA-type matrix element $\bar{v}$, whose magnitude squared is to be averaged over the possibly excited configuration. Energy is conserved at each step.

Since each factor in (5.29) is forward peaked, one may expect the multistep angular distribution to be forward peaked but generally broader than that of the single step, reflecting the number of stages contributing significantly.

Problem. Assume that each factor in (5.29) is a function of the momentum transfer, $\mathbf{k}_\nu - \mathbf{k}_{\nu-1}$, occurring at step. Evaluate the integral in (5.29), showing that it has the form

$$\int e^{i\gamma_f\cdot(\mathbf{k}_f - \mathbf{k}_i)} \prod_1^\mu f_\nu(\gamma_f)\, d\gamma_f$$

where

$$\frac{d^2 w(\mathbf{k}_\nu, \mathbf{k}_{\nu-1})}{d\Omega_\nu\, dU_\nu} = \int e^{i\gamma_\nu\cdot(\mathbf{k}_\nu - \mathbf{k}_{\nu-1})} f_\nu(\gamma_\nu)\, d\gamma_\nu$$

Show from this result that the integral in (5.29) will have a broader angular distribution than that given by the individual step.

B. Statistical Multistep Compound Reactions

The separation of the $\mathscr{T}$ matrix into a direct term and a fluctuating one with vanishing average value using the results of Kawai, Kerman, and McVoy (73) has been discussed in Section IV.8. The direct reactions described by the direct term have been the subject of the discussion in the chapter up to this point.

We turn now to a consideration of the fluctuating term, which has its origin in the Q-subspace chain of Fig. 5.2. Equation (IV.8.8) gives the $\mathscr{T}$ matrix for that case:

$$\mathscr{T}_{fi}^{(\mathrm{msc})} = \left\langle \phi_f^{(-)} V_{PQ} \frac{1}{E - h_{QQ}} V_{QP} \phi_i^{(+)} \right\rangle \tag{5.33}$$

where

$$h_{QQ} = H_{QQ} + V_{QP} \frac{1}{E^{(+)} - H_{\mathrm{opt}}} V_{PQ} \tag{5.34}$$

V_{PQ} is defined by (IV.8.6), H_{QQ} equals QHQ, and H_{opt} is the multichannel optical model Hamiltonian. We see that the effect of the P subspace is included in h_{QQ} through its dependence on H_{opt}.

The analysis of $\mathscr{T}_{fi}^{(\mathrm{msc})}$ given by (5.33) parallels completely that of $\mathscr{T}_{fi}^{(\mathrm{msd})}$ following (5.11). First one can write $\mathscr{T}_{fi}^{(\mathrm{msc})}$ as a linear combination of amplitudes coming from each stage:

$$\mathscr{T}_{fi}^{(\mathrm{msc})} = \sum_{1}^{r} \mathscr{T}_{fi}^{(m)} \tag{5.35}$$

where

$$\mathscr{T}_{fi}^{(m)} = \left\langle \phi_f^{(-)} V_{PQ_m} \frac{1}{E - h_{QQ}} V_{Q_1 P} \phi_i^{(+)} \right\rangle \tag{5.36}$$

where

$$V_{PQ_m} \equiv PVQ_m$$

and Q_m is the projection operator for subspace Q_m. As in (5.14),

$$Q_k \frac{1}{E - h_{QQ}} Q_1 = G_k V_{k,k-1} G_{k-1} \frac{1}{E - h_{QQ}} Q_1 \tag{5.37}$$

where

$$V_{k,k-1} \equiv Q_k V Q_{k-1}$$

and

$$G_k = \frac{1}{E - h_{kk} - V_{k,k+1} G_{k+1} V_{k+1,k}} \tag{5.38}$$

[see (5.16)].

Note that the sum over m in (5.35) terminates at $m = r$, so that $G_r = (E - h_{rr})^{-1}$.

Equation (5.37) is now to be inserted in (5.36). One obtains

$$\mathscr{T}_{fi}^{(m)} = \langle \phi_f^{(-)} V_{Pm} G_m V_{m,m-1} G_{m-1} \cdots V_{21} G_1 V_{1P} \phi_i^{(+)} \rangle \tag{5.39}$$

[Compare with (5.11)]. Recall that

$$Q_k \Psi_i^{(+)} = Q_k \frac{1}{E - h_{QQ}} V_{1P} \phi_i^{(+)}$$

where the left-hand side gives the component in space Q_k of the exact solution of the Schrödinger equation for the system. Using (5.37) yields

$$Q_k \Psi_i^{(+)} = G_k V_{k,k-1} Q_{k-1} \Psi_1^{(+)} \tag{5.40}$$

so that (5.39) can be written as follows:

$$\mathcal{T}_{fi}^{(m)} = \langle \phi_f^{(-)} V_{Pm} G_m V_{m,m-1} Q_{m-1} \Psi_i^{(+)} \rangle \tag{5.41}$$

We need to calculate the energy average of $|\mathcal{T}_{fi}^{(m)}|^2$. Rapid variations in the energy dependence of $\mathcal{T}_{fi}^{(m)}$ is assumed to originate in the propagators G_k. From (5.38) we see that an implicit source of energy dependence is given by the term $V_{k.k+1} G_{k+1} V_{k+1,k}$. We shall now describe one set of circumstances (verifiable in a detailed calculation) under which the energy dependence of this term can be neglected. The inverse of G_{k+1} will have eigenfunctions and eigenvalues given by

$$G_{k+1}^{-1} \psi_{k+1,\alpha} = \varepsilon_{k+1,\alpha} \psi_{k+1,\alpha} \tag{5.42}$$

and

$$(G_{k+1}^{-1})^{\dagger} \tilde{\psi}_{k+1,\alpha} = \varepsilon_{k+1,\alpha}^{*} \tilde{\psi}_{k+1,\alpha} \tag{5.43}$$

Since G_{k+1} is not generally Hermitian, the eigenvalue $\varepsilon_{k+1,\alpha}$ will be complex:

$$\varepsilon_{k+1,\alpha} = E_{k+1,\alpha} - i \frac{\Gamma_{k+1,\alpha}}{2} \tag{5.44}$$

In terms of these eigenfunctions,

$$w_{kk} \equiv V_{k,k+1} G_{k+1} V_{k+1,k} = \sum_{\alpha} V_{k,k+1} \psi_{k+1,\alpha} \rangle \frac{1}{E - \varepsilon_{k+1,\alpha}} \langle \tilde{\psi}_{k+1,\alpha}$$

We see that the energy dependence of w_{kk} will be smooth over the energy variation given by $\Gamma_{k+1,\alpha}$. For the purpose of energy averaging and employing the random phase approximation, it is necessary that many states $\psi_{k,\beta}$ be continued in that interval, leading to the condition

$$\rho_k \Gamma_{k+1} \gg 1 \qquad \text{or} \qquad \Gamma_{k+1} \gg D_k \tag{5.45}$$

where ρ_k is the density of levels in kth subspace, D_k the energy spacing, and

Γ_{k+1} the average value of $\Gamma_{k+1,\alpha}$. Under this condition, *self-averaging* takes place. The condition is equivalent to the statement that the Poincaré time for the kth stage is large compared to the lifetime of the states in the $(k+1)$st stage. Condition (5.45) can be checked by direct calculation. In the examples to be described, the condition is well satisfied.

Assuming (5.45), it becomes possible to expand G_m in (5.41) in a spectral series so that

$$\mathscr{T}_{fi}^{(m)} = \sum \langle \phi_f^{(-)} V_{Pm} \psi_{m,\alpha} \rangle \frac{1}{E - \varepsilon_{m\alpha}} \langle \tilde{\psi}_{m,\alpha} V_{m,m-1} Q_{m-1} \Psi_i^{(+)} \rangle \tag{5.46}$$

when $\varepsilon_{m\alpha}$ varies slowly with energy.

Problem. Prove that the energy average of $\mathscr{T}_{fi}^{(m)}$ is zero.

To obtain the cross section we need to compute the energy average of $|\mathscr{T}_{fi}^{(\mathrm{msc})}|^2$:

$$|\mathscr{T}_{fi}^{(\mathrm{msc})|2} = \sum_{mm'} (\mathscr{T}_{fi}^{(m')})^* (\mathscr{T}_{fi}^{(m)}) \to \sum_m |(\mathscr{T}_{fi}^{(m)})|^2$$

where the random-phase approximation is used to obtain the last expression. Using (5.46) yields

$$|\mathscr{T}_{fi}^{(m)}|^2 = \sum_{\alpha\beta} \langle \phi_f^{(-)} V_{Pm} \psi_{m,\alpha} \rangle \frac{1}{E - \varepsilon_{m\alpha}} \langle \tilde{\psi}_{m,\alpha} V_{m,m-1} Q_{m-1} \Psi_i^{(+)} \rangle$$

$$\times \langle \phi_f^{(-)} V_{Pm} \psi_{m,\beta} \rangle^* \frac{1}{E - \varepsilon_{m\beta}^*} \langle \tilde{\psi}_{m,\beta} V_{m,m-1} Q_{m-1} \Psi_i^{(+)} \rangle$$

Again because of the random-phase approximation the double sum can be collapsed to a single sum since only the $\alpha = \beta$ terms survive. Therefore,

$$|\mathscr{T}_{fi}^{(m)}|^2 = \sum_\alpha |\langle \phi_f^{(-)} V_{Pm} \psi_{m\alpha} \rangle|^2 \frac{1}{|E - \varepsilon_{m\alpha}|^2} |\tilde{\psi}_{m,\alpha} V_{m,m-1} Q_{m-1} \Psi_i^{(+)} \rangle|^2$$

The energy average is taken assuming that only the variation of the energy denominator is important and that the energy variation of the matrix elements is slow, so that their magnitude squared can be replaced by an average value over the set $\psi_{m\alpha}$. The result is

$$\langle |\mathscr{T}_{fi}^{(m)}|^2 \rangle = \frac{\Gamma_m^{(f)}}{\Gamma_m} \frac{\langle |\langle \tilde{\psi}_{m,\alpha} V_{m,m-1} Q_{m-1} \Psi_i^{(+)} \rangle|^2 \rangle}{D_m} \tag{5.47}$$

Where

$$\Gamma_m^{(f)} \equiv 2\pi \langle |\phi_f^{(-)} V_{Pm} \psi_{m\alpha} \rangle|^2 \rangle \tag{5.48}$$

is referred to as the escape width. One now uses (5.40) again on the remaining factor in (5.47), to obtain

$$\langle|\mathscr{T}_{fi}^{(m)}|^2\rangle = \frac{\Gamma_m^{(f)}}{\Gamma_m}\cdot\frac{\Gamma_{m-1}^{\downarrow}}{\Gamma_{m-1}}\frac{\langle|\langle\tilde{\psi}_{m-1,\alpha}V_{m-1,m-2}Q_{m-2}\Psi_i^{(+)}\rangle|^2\rangle}{D_{m-1}}$$

where

$$\Gamma_{m-1}^{\downarrow} = \frac{2\pi}{D_m}\langle|\langle\tilde{\psi}_{m,\alpha}V_{m,m-1}\psi_{m-1,\beta}\rangle|^2\rangle \tag{5.49}$$

is referred to as the *spreading width.* The averages are over the states in the mth and $(m-1)$st subspaces. Iterating, one obtains

$$\langle|\mathscr{T}_{fi}^{(m)}|^2\rangle = \frac{1}{(2\pi)^2}\frac{\Gamma_m^{(f)}}{\Gamma_m}\prod_{k=1}^{m-1}\frac{\Gamma_k^{\downarrow}}{\Gamma_k}\cdot\frac{2\pi\Gamma_1^{(i)}}{D_1} \tag{5.50}$$

where

$$\Gamma_1^{(i)} = 2\pi\langle|\langle\psi_{1\alpha}V_{1P}\phi_i^{(+)}\rangle|^2\rangle \tag{5.51}$$

Therefore

$$\langle|\mathscr{T}_i^{(\mathrm{msc})}|^2\rangle = \frac{1}{(2\pi)^2}\sum_{m=1}^{r}\frac{\Gamma_m^{(f)}}{\Gamma_m}\left[\prod_{k=1}^{m-1}\frac{\Gamma_k^{\downarrow}}{\Gamma_k}\right]\frac{2\pi\Gamma_1^{(i)}}{D_1} \tag{5.52}$$

It is convenient to normalize $\phi_i^{(+)}$ and $\phi_f^{(-)}$ so that the widths have the dimension of an energy and $\mathscr{T}$ is dimensionless. This is the case if the normalization is per unit energy. The cross section for a given channel with quantum numbers designated by γ is given by

$$\sigma_{fi}^{(\mathrm{msc})} = \frac{\pi}{k^2}\sum_{m=1}^{r}\frac{\Gamma_m^{(f)}}{\Gamma_m}\left[\prod_{1}^{m-1}\frac{\Gamma_k^{\downarrow}}{\Gamma_k}\right]\frac{2\pi\Gamma_1(i)}{D_1} \tag{5.53}$$

while the expression for the angular distribution is given by (5.55′).

Equation (5.52) can be described as a product of factors with relatively simple meaning. The first $(2\pi\Gamma_i^{(i)}/D_1)$ is the strength function measuring the probability of the system making the transition from the incident channel to the first subspace Q_1. This is followed by a product that measures the attenuation because of emission en route to the mth channel and finally, the branching ratio for emission from the mth subspace. the total widths Γ_k are generallly not the sum of the escape and spreading widths [see Feshbach, Kerman, and Koonin (80)] except in the case of weak coupling between the P and Q spaces.

Finally, it is necessary to average $d\sigma_\gamma^{(\mathrm{msc})}/dU$ over the final states since experimentally it is not possible to distinguish among them. The final wave function $\phi_f^{(-)}$ in (5.48) for $\Gamma_m^{(f)}$ is composed of contributions from all stages, P_μ. However, because of the chaining hypothesis, the states in subspace Q_m can

make transitions only to P_m, P_{m-1}, and P_{m+1}. Assuming that the coupling among the various P_μ spaces is strong, the wave function $\phi_f^{(-)}$ will be "well mixed", so that to a good approximation the probability of the component of $\phi_f^{(-)}$ being in subspace of P_μ is given by $\rho_\mu^{(\gamma)}(U)/\rho^{(\gamma)}(U)$ when $\rho_\mu^{(\gamma)}$ is the density of the states in subspace P_μ with channel quantum numbers symbolized by γ, and $\rho^{(\gamma)}(U)$ is the total density of channels of the type γ at the excitation energy U:

$$\rho^{(\gamma)}(U) = \sum_\mu \rho_\mu^{(\gamma)}(U)$$

With this assumption

$$\Gamma_m^{(\gamma)} = \sum_{\mu=m-1}^{m+1} \frac{\rho_\mu^{(\gamma)}(U)}{\rho^{(\gamma)}(U)} \Gamma_{m\mu}^{(\gamma)}(U) \tag{5.54}$$

where $\Gamma_{m\mu}^{(\gamma)}$ is given by

$$\Gamma_{m\mu}^{(\gamma)} = 2\pi \langle | \langle \chi_{\mu\beta}^{(-)} V_{Pm} \psi_{m\alpha} \rangle |^2 \rangle$$

where $\chi^{(-)}$ is given by (5.22). The average is taken over the indices β and α.

We can now average $\sigma_f^{(\mathrm{msc})}$ over a small energy interval dU, where U is the excitation energy of the residual nucleus. The right-hand side of (5.53) is multiplied by $\rho^{(\gamma)}(U)\,dU$ and $\Gamma_m^{(J)}$ is replaced by its average value, $\rho_\mu^{(\gamma)}(U)\Gamma_{m\mu}^{(\gamma)}(U)/\rho^{(\gamma)}(U)$. We thus finally obtain

$$\frac{d\langle \sigma_\gamma^{(\mathrm{msc})} \rangle}{dU} = \frac{\pi}{k^2} \sum_{m=1}^{r} \sum_{\mu=m-1}^{m+1} \frac{\langle \rho_\mu^{(\gamma)}(U)\Gamma_{m\mu}^{(\gamma)}(U) \rangle}{\Gamma_m} \left[\sum_1^{m-1} \frac{\Gamma_k^{\downarrow}}{\Gamma_k} \right] \frac{2\pi\Gamma_1^{(i)}}{D_1} \tag{5.55}$$

The channel parameters γ are, for example, those used in Section 2: namely, channel spin S, critical angular momentum l, and total angular momentum J. The angular distribution is obtained in the standard way, with the result.

$$\frac{d^2\sigma}{d\Omega\, dU} = \sum \frac{(-)^{S-S'}}{(2I+1)(2i+1)} \bar{Z}(lJlJ; SL)\bar{Z}(l'Jl'J; S'L) P_L(\cos\vartheta) \frac{d\sigma_\gamma^{(\mathrm{msc})}}{dU} \tag{5.55'}$$

where

$$\bar{Z}(lJlJ; SL) = (-)^{s+J+L}(lsJ \,\|\, Y_L \,\|\, lSJ)$$
$$= 0 \quad \text{unless } L \text{ is even}$$

Formula (5.55) appears to be similar to that used in the preequilibrium theories reviewed, for example, by Blann (72). It is not identical, as the latter refer to the angle integrated cross section and do not predict angular distributions. Because of the random-phase approximation, the statistical

multistep compound reaction cross section is symmetric about 90°. Note finally that (5.55) automatically contains the compound nuclear contribution to the cross section given by the rth term in (5.55).

Because of the preliminary stages through which the system has to pass before arriving at the statistical compound state, the Bohr independence hypothesis and its consequence the statistical reaction theory (Hauser–Feshbach) must be modified. This is seen most readily if we return to (5.55) and examine just the compound nuclear term, the rth term:

$$\sigma_{fi,r}^{(\mathrm{msc})} = \frac{\pi}{k^2} \frac{\Gamma_r^{(f)}}{\Gamma_r} \prod_1^{r-1} \frac{\Gamma_k^{\downarrow}}{\Gamma_k} \cdot \frac{2\pi\Gamma_1^{(i)}}{D_1} \tag{5.56}$$

Since the Q_r subspace is the last subspace in the chain, Γ_r is equal to the escape width:

$$\Gamma_r = \Gamma_r^{\uparrow} = \sum_c \Gamma_r^{(c)} \tag{5.57}$$

where the sum is over all possible final states. Let the transmission factor T_c be given by

$$T_c \equiv \frac{2\pi\Gamma_r^{(c)}}{D_r}$$

Then

$$\sigma_{fi,r}^{(\mathrm{msc})} = \frac{\pi}{k^2} \frac{T_f T_i}{\Sigma_c T_c} \tag{5.58}$$

The factor T_i is

$$T_i \equiv 2\pi \frac{\Gamma_1^{(i)}}{D_1} \prod_{k=1}^{r-1} \frac{\Gamma_k^{\downarrow}}{\Gamma_k} \tag{5.59}$$

Although (5.58) is similar to the Hauser–Feshbach expression, it can differ substantially because of the presence of the depletion factor, that is,

$$\sigma_{fi,r}^{(\mathrm{msc})} = \sigma_{\mathrm{HF}} \prod_{k=1}^{r} \frac{\Gamma_k^{\downarrow}}{\Gamma_k} \tag{5.60}$$

Here σ_{HF} is the Hauser–Feshbach expression. Moreover, since the depletion factor depends on the nature of the entrance channel, which determines the quantification of complexity and therefore the partition of Hilbert space in P and Q and of Q into Q_μ, the Bohr independence hypothesis is violated.

One interesting sum rule can be obtained from (5.53). Sum this cross section over all possible final states to obtain the total reaction cross section, σ:

$$\sigma = \sum_f \sigma_{fi}^{(\mathrm{msc})} = \frac{\pi}{k^2} \sum_{m=1}^{r} \frac{\Gamma_m^{\uparrow}}{\Gamma_m} \left[\prod \frac{\Gamma_k^{\downarrow}}{D_1} \right] \frac{2\pi\Gamma_1^{(i)}}{D_1} \tag{5.61}$$

If now one makes the weak PQ coupling approximation

$$\Gamma_\mu = \Gamma_\mu^{\uparrow} + \Gamma_\mu^{\downarrow}$$

(5.61) reduces to

$$\sigma = \frac{\pi}{k^2} \frac{2\pi\Gamma_1^{(i)}}{D_1} \tag{5.62}$$

Thus the total reaction cross section is proportional to the strength function for the formation of doorway states in subspace Q_1.

6. APPLICATIONS

The results of Section 5 [Eqs. (5.29) and (5.55)] have been applied to the analysis of experiments in which the incident and emerging particles are nucleons, such as (p, p'), (n, n'), (p, n), (n, p), and $(\mathbf{p}, n)$. Projectile energies range from 14 to 65 MeV, while a variety of target nuclei, including medium heavy as well as heavy nuclei, were used. There have been a few calculations carried out for ^{3}He- and ^{4}He-induced reactions [Bonetti, Colli-Milazzo, and Melanotte (81)]. Generalizations have been developed (and explained) which are appropriate for the study of reactions with multiparticle final states [Feshbach (79); Ciangaru, Chang, et al. (84); Field, Bonetti, and Hodgson (85)].

The calculations for nucleon induced reactions have been carried out by Colli-Milazzo, Bonetti, Hodgson, and their colleagues in more than a dozen papers [de Rosa, Inglima, et al. (78); Bonetti, Caninasio, Colli-Milazzo, and Hodgson (81); Bonetti, Colli-Milazzo, and Melanotte (81a, 81b, 83); Bonetti, Colli-Milazzo, et al. (80, 82a, 82b); Bonetti and Columbo (83); Avaldi et al. (80); Austin et al. (80), Field et al. (86) Holler et al. (85)]. It is not possible to describe the details involved in these many analyses. We shall give some examples of the results obtained, together with the principal conclusions.

The elements that enter into the calculation include the residual potential responsible for the transition between stages, the bound-state wave functions, and the wave functions for the particle in a continuum state. The choice is guided by the standard DWA results. In the more precise calculations, the residual interaction is taken to be a Yukawa potential. Distorted waves for the continuum and the bound-state wave function are obtained using a Woods–Saxon potential selected in accord with elastic scattering and single-step

DWA results available in the energy range and for the target of interest. Overall good agreement with experiment, illustrated below, was obtained with *identical* residual interactions employed in all cases: target nuclei, excitation energy and angle, and for both statistical multistep direct and compound reactions. That strength between unlike nucleons is taken to be 27 MeV with a range of 1 fm [Bonetti and Columbo (83), Bonetti, Colli-Milazzo, and Melanotte (81a)]. Rough calculations have also been made for the statistical multistep compound reaction with δ function residual potential and constant bound-state wave functions. It turns out that the effect of these approximations on the energy spectra and angular distributions is small.

In each situation it is necessary to choose a path in reaction space; that is, what are the stages in which the system can be found? For example, in the (p, n) statistical multistep direct case {Bonetti, Colli-Milazzo, and Melanotte (81a)], the first stage is generated by a charge exchange scattering with the formation of a proton–particle–neutron–hole in the target nucleus plus a neutron in the continuum. The more complex states, P_n, involve np–nh states with a neutron in the continuum. Clearly, there are many other possibilities. For example, the charge exchange scattering could be postponed to a later stage.

The sensitivity of the results to the various paths in reaction space has not been studied systematically. However, Bonetti, Colli-Milazzo, and Melanotte (81a) found that for their several cases they need not distinguish between the neutrons and protons provided that an averaged interaction strength is used and except for the initial and final step. Chao, Hachenberg, and Hüfner (82) have emphasized the importance of the first step and suggest a relative insensitivity to the nature of the succeeding stages.

The density of particle–hole states required in both SMC and SMD processes is given by the Ericson (60c) expression. We give a simple derivation of the result. One assumes a constant density g of single-particle states; that is, the probability that a particle has an energy between x and $x + dx$ is $g\,dx$. Then the probability that p particles and h holes ($N = p + h =$ exciton number) have an excitation energy E is

$$\rho_{\mathrm{ph}}(E) = \frac{1}{p!\,h!}\int_0^\infty dx_1 \cdots dx_p \int_0^\infty dy_1 \cdots dy_k g^{p+h}\delta\left(E - \sum_1^p x_i - \sum_1^h y_i\right) \tag{6.1}$$

where we have assumed that g is a constant, an assumption which can be easily modified. Replacing the δ function by its integral representation

$$\delta\left(E - \sum_1^p x_i - \sum_1^h y_i\right) = \frac{1}{2\pi}\int_{-\infty}^{\infty} dk\, e^{ik(E - \sum x_i - \sum y_i)}$$

Equation (6.1) becomes

$$\rho_{\mathrm{ph}}^{(N)}(E) = \frac{1}{2\pi}\frac{g^N}{p!\,h!}\int_{-\infty}^{\infty} dk\, e^{ikE}\left(\int_0^\infty dx\, e^{-ikx}\right)^p\left(\int_0^\infty dy\, e^{-iky}\right)^h$$

For the x and y integrals to be convergent, the path of the k integration must lie in the lower half of the complex k plane. One obtains

$$\rho_{\mathrm{ph}}^{(N)}(E) = \frac{1}{2\pi}\frac{g^N}{p!\,h!}\int_{-\infty}^{\infty} dk\,\frac{e^{ikE}}{(ik)^N}$$

Using the Cauchy integral formula yields the Ericson result,

$$\rho_{\mathrm{ph}}^{(N)}(E) = \frac{g(gE)^{N-1}}{p!\,h!\,(N-1)!} \tag{6.2}$$

To obtain the density of particle–hole states formed from single-particle states of a given J, one must multiply (6.2) by spin distribution function (IV.5.54), yielding

$$\rho_{\mathrm{ph}}^{(N)}(E,J) = \rho_{\mathrm{ph}}^{(N)}(E)R_N = \frac{g(gE)^{N-1}}{p!\,h!\,(N-1)!}\,\frac{2J+1}{\sqrt{8\pi}\sigma^3 N^{3/2}}\,e^{-(J+1/2)^2/2N\sigma^2} \tag{6.3}$$

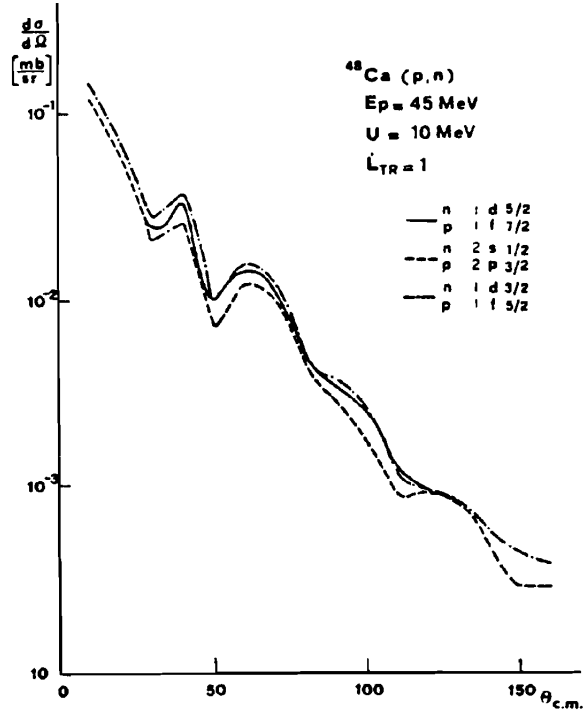

FIG. 6.1. Calculated differential cross sections for some typical transitions in ^{48}Ca at 45 MeV between shell model states corresponding to $\Delta L = 1$, showing their overall similarity. [From Bonetti, Camnasio et al. (81).]

In the shell-model basis, the states in stage $n+1$ differ from those in stage n by a particle–hole excitation; that is, $N=2$, $p=1$, and $h=1$.

The average of the square matrix elements is given by

$$\langle|\bar{v}(\mathbf{k}_i,\mathbf{k}_f)|^2\rangle=\sum_L(2L+1)\langle|\bar{v}(\mathbf{k}_i,\mathbf{k}_f,L|^2\rangle R_2(L)$$

and

$$\left\langle\left[\frac{d^2\sigma(\mathbf{k}_i,\mathbf{k}_f)}{dU\,d\Omega}\right]_{\text{single step}}\right\rangle=\sum_L(2L+1)\rho^{(2)}(E)R_2(L)\left\langle\left(\frac{d\sigma}{d\Omega}\right)\right\rangle_L$$

in the case that the spin of the target is zero and if the spin of the nucleons is neglected (then $J=L$). The average over $(d\sigma/d\Omega)_L$ for various possible values of the particle–hole angular momenta is readily accomplished because of the similarity of the results for each of the possibilities. This is illustrated by Fig. 6.1.

Some results that illustrate the degree of agreement with experiment will now be presented. Note that in all cases the log of the cross section is plotted. Figures 6.2 to 6.5 compare the results of a multistep direct calculation of the

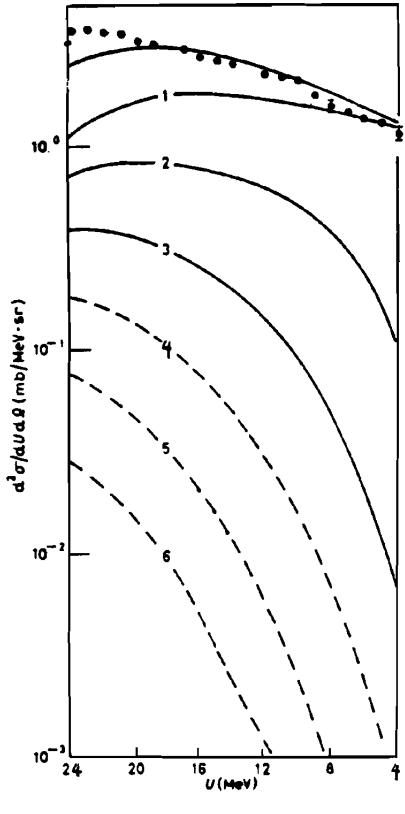

FIG. 6.2. Neutron energy spectrum for the reaction $^{120}\text{Sn}(p,n)$, $E_p=45$ MeV $\theta_{\text{cm}}=30°$. The black dots are the experimental points; the solid line the calculated results. The numerical labels correspond to the number of steps. [From Avaldi, Bonetti, and Colli-Milazzo (80).]

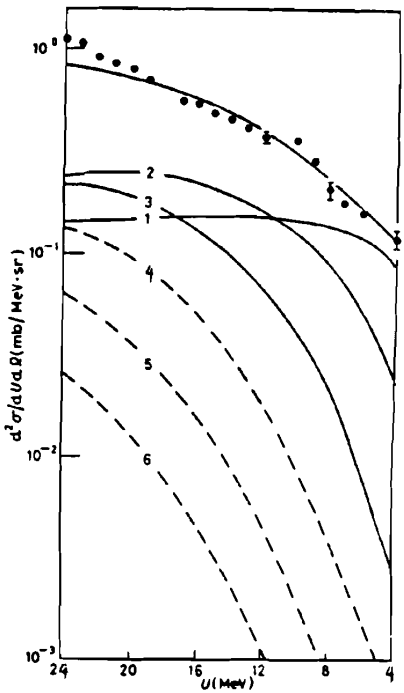

FIG. 6.3. Neutron energy spectrum for the reaction $^{120}\mathrm{Sn}(p,n)$, $E_p = 45$ MeV $\theta_{cm} = 90°$ (see legend for Fig. 6.2). [From Avaldi, Bonetti, and Colli-Milazzo (80).]

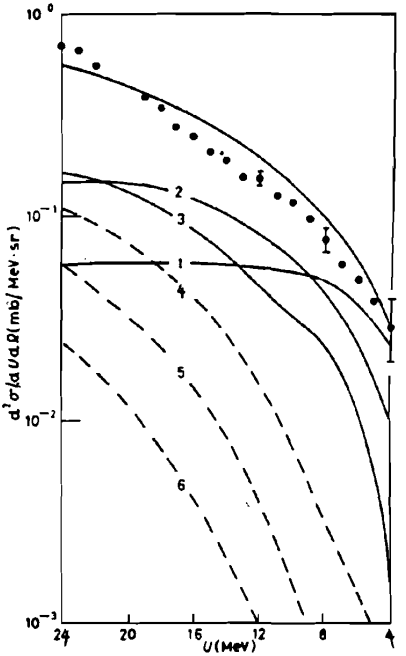

FIG. 6.4. Neutron energy spectrum for the reaction $^{120}\mathrm{Sn}(p,n)$, $E_p = 45$ MeV $\theta_{cm} = 120°$ (see legend for Fig. 6.2). [From Avaldi, Bonetti, and Colli-Milazzo (80).]

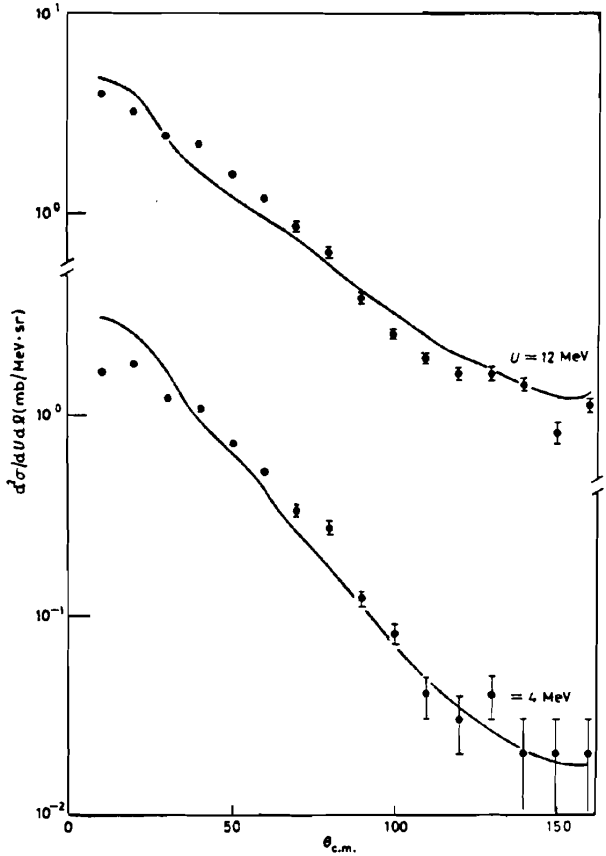

FIG. 6.5. Neutron angular distribution for the reaction ^{120}Sn(p, n), $E_p = 45$ MeV. The solid lines are calculated results. [From Avaldi, Bonetti, and Colli-Milazzo (80).]

Sn(p, n) cross sections for 45-MeV protons [Avaldi, Bonetti, and Colli-Milazzo (80)]. Good agreement is obtained. There is some deviation at low neutron energies, where there is a contribution from the multistep compound process not included in the calculation. We note that the single-step process gives accurate results only with a low excitation energy of the residual nucleus and in the forward direction. But as the excitation energy increases and/or the emission angle increases, the contribution of the two-step and then the three-step process becomes important. No more than three steps are required in the angular range beyond 150°. The calculated angular distribution shown in Fig. 6.5 matches experiment throughout the angular range. Similar calculations have been performed for a (p, n) reaction, proton energy 45 MeV, for a number of nuclei [Bonetti, Colli-Milazzo, and Melanotte (81a)] with similar success. The need to include contributions from the SMC process as the proton energy decreases is shown in Fig. 6.6.

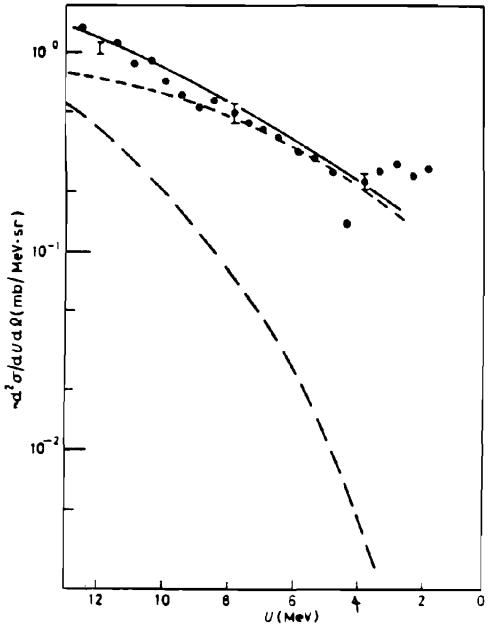

FIG. 6.6. Neutron energy spectrum for the reaction ^{120}Sn$[p, n)$ $E_p = 25$ MeV, $\theta_{cm} = 110°$; ————, total; ———, multi step direct, – – – –, multistep compound. [From Colli-Milazzo private communication quoted in Feshbach (86).]

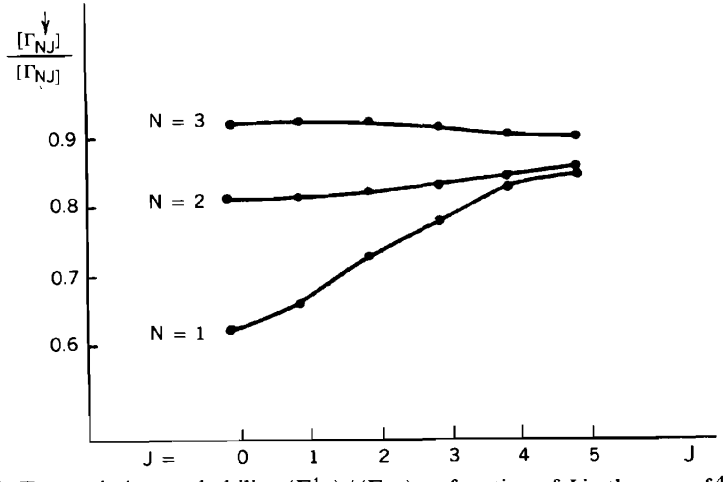

FIG. 6.7. Transmission probability $\langle\Gamma^1_{NJ}\rangle/\langle\Gamma_{NJ}\rangle$ as function of J in the case of ^{40}Ca(n, p) [From Bonetti, Colli-Milazzo, and Melanotte (83).]

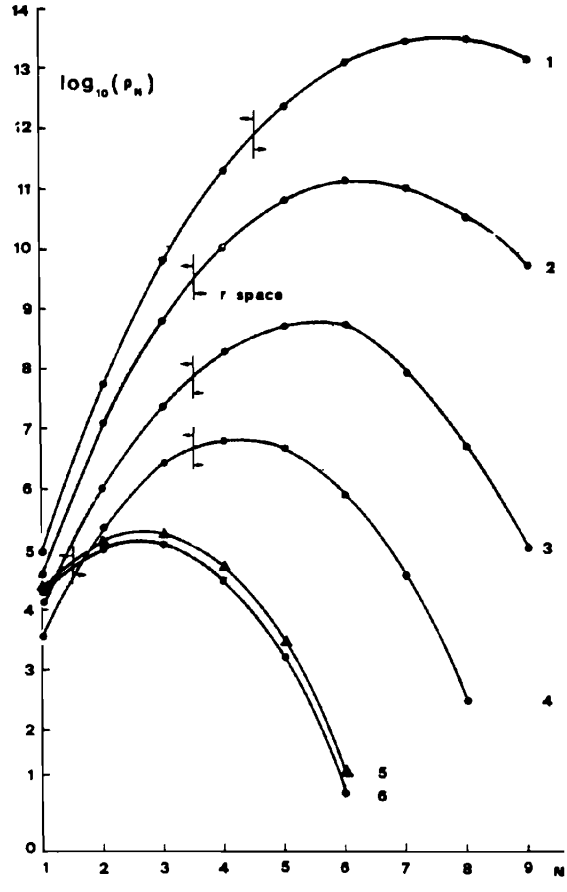

FIG. 6.8. Level density of the various composite nuclei as a function of the stage N of the precompound chain: (1) ^{104}Pd, (2) ^{90}Zr, (3) ^{60}Ni, (4) ^{41}Ca, (5) ^{30}P, and (6) ^{28}Si. [From Bonetti, Colli-Milazzo, and Melanotte (83).]

We turn next to some examples of the statistical multistep compound (SMC) reactions. "Equilibrium" sets in at about the fourth step, as indicated by Fig. 6.7, where we see that by the third step the branching ratio to the fourth step is approximately 0.9. Note that the level density at the fourth stage is on the order of 10 times that at the third stage (see Fig. 6.8), so that the self-averaging condition of Tang Xuetian (81) is well satisfied. It is important in the SMC calculations to include only bound orbits, as emphasized by Bonetti, Colli-Milazzo, and Melanotte (83). Two examples are shown, In Fig. 6.9 a comparison is made between experiment and theory for the ^{51}V$(p,n)^{51}$Cr reaction, for a proton energy of 22 MeV. We see the striking failure of the evaporation model and the good agreement that is obtained when the SMC theory, which takes into account the emission that occurs before the equilibra-

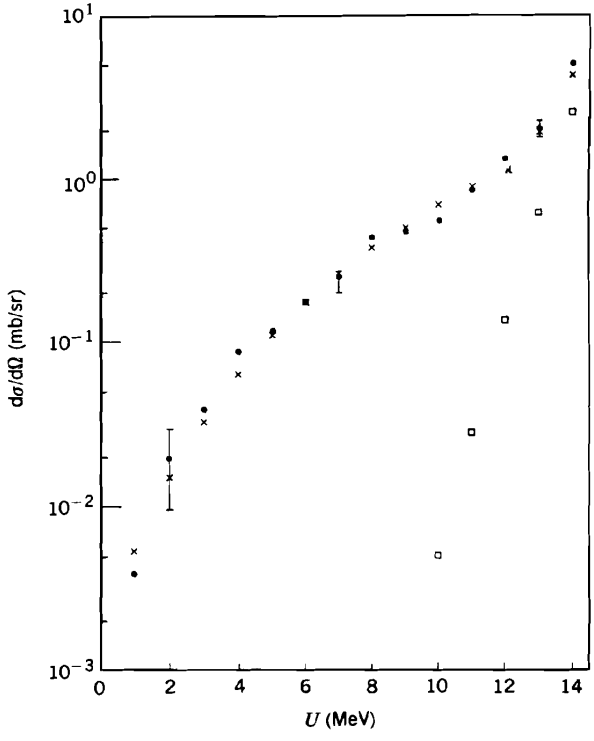

FIG. 6.9. Double differential spectrum for the reaction $^{51}V(p,n)^{51}Cr$, $E_p = 22$ MeV, $\theta = 144°$. Experimental points from Grimes, Anderson, et al. (71) are given by circles, the calculated evaporation spectrum by the squares, and the total statistical multistep compound by the crosses. [From Feshbach, Kerman, and Koonin (80).]

tion (rth) stage, is reached. In Fig. 6.10 a comparison is made for the case of 14-MeV neutrons incident on ^{93}Nb, including the (n,n'), $(n,2n)$, and (n,pn) contributions. The dashed line gives the contribution from the rth stage (the evaporation component) for (n,n'), the dotted line for the $(n,2n)$ and (n,pn).

The behavior of parameters of the SMD theory is shown in Table 6.1. In this table σ is the spin cutoff parameter, $6a/\pi^2$ gives single-particle density g, V_0 is the strength of the Yukawa potential with a range of 1 fm [used for the residual $(p-n)$ potential], $\bar{V}_0$ is the strength averaged over the $p-n$ and $n-n$ interaction strengths, and finally, the ratio of the single-step cross section to the total is shown. Bonetti and Columbo (83) show that the strength of the potentials used in the SMC is consistent with that given by the table.

The statistical multistep direct theory has also been employed to predict the inelastic scattering of 65-MeV polarized protons by ^{58}Ni [Bonetti, Colli-Milazzo, et al. (82b)]. Comparisons with the measurements of Sakai, Hosono, et al. (80) show excellent agreement with the angular distributions and

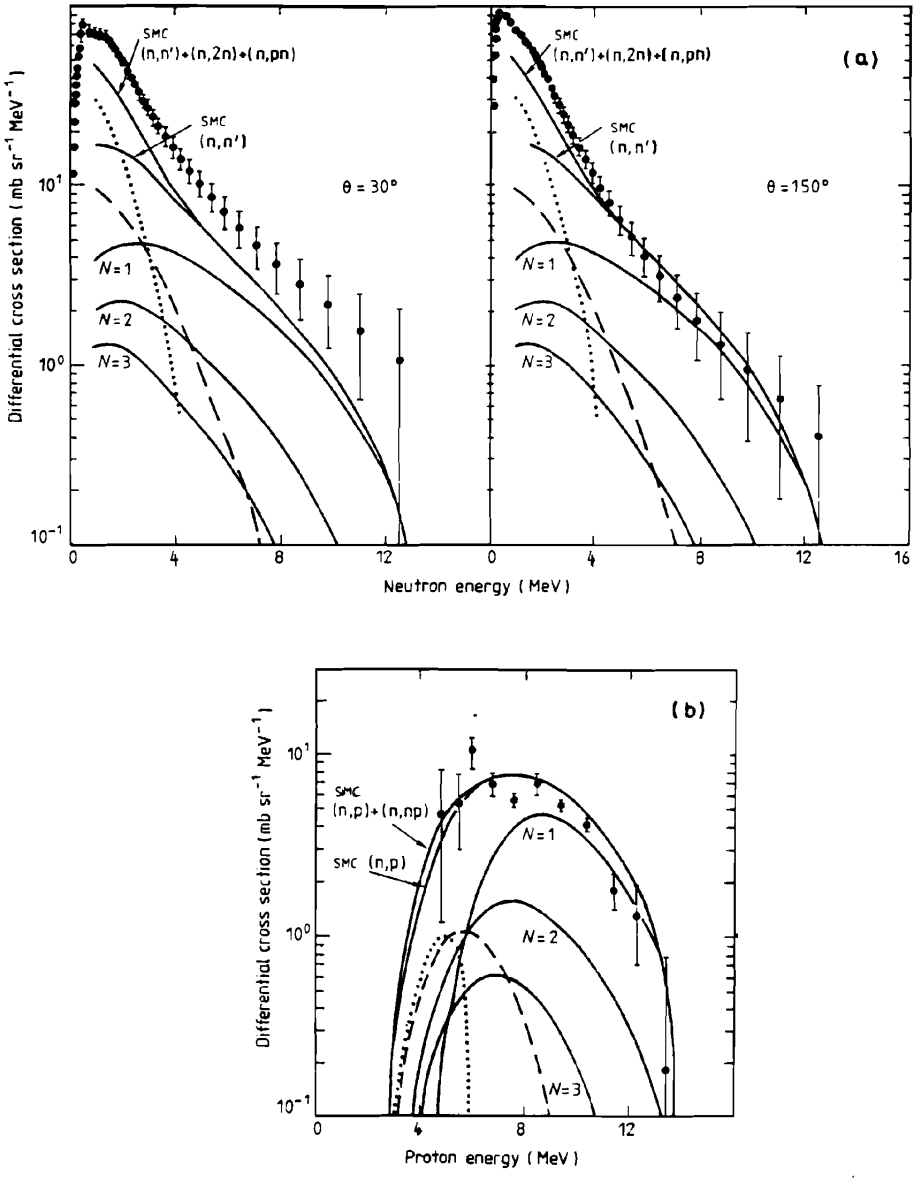

FIG. 6.10. (*a*) Energy spectrum of neutrons emitted at 30° and 150° from ^{93}Nb at an incident neutron energy of 14 MeV. The experimental data of Salnikov, Lovchikova et al. (70, 71) are compared with the statistical multistep compound calculations. (*b*) Energy spectrum of protons emitted at 150° from ^{93}Nb at an incident neutron energy of 14 MeV. The experimental data of Grimes, Anderson, et al. (78) are compared to statistical multi step compound calculations. For both (a) and (b) the curves labeled with N show the contributions of the N-step process. The dashed and dotted lines give the contributions of r stage processes which for case (*a*) are (n,n') and $(n,2n)+(n,pn)$, respectively; for (*b*) they are (n,p) and (n,np), respectively. [From Field, Bonetti, and Hodgson (86).]

TABLE 6.1

Target	σ	$a(=\pi^2/6g)(\text{MeV}^{-1})$	V_0(MeV)	$\bar{V}_0$(MeV)	σ_1/σ_{tot}
^{48}Ca(E_p=45 MeV)	1	7.4	27.5	15.5	0.55
^{90}Zr(E_p=45 MeV)	1.4	10	27.5	17	0.55
^{120}Sn(E_p=25 MeV)	1.8	16	27.5	16	0.82
^{129}Sn(E_p=35 MeV)	1.8	16	27.5	16	0.72
^{208}Pb(E_p=45 MeV)	2.4	13	27	15	0.47

Source: Bonetti and Colambo (83).

analyzing power. Agreement with the latter is good only for relatively low excitation, $U = 10$ and 14 MeV but fails in the intermediate angular range $45° < \vartheta < 110°$ for $U = 18$ and 22 MeV. Presumably, the inclusion of the MSC process is needed for these large excitation energies.

A number of conclusions can be drawn from this analysis: The division of the statistical reaction process into multistep direct and multistep compound components appears to be useful and important. The multistep direct process dominates at the higher projectile energies, while the multistep compound is important for large excitation energies of the residual nucleus as well as for lower projectile energies. At sufficently low energies the system is "trapped" on the first step so that there is no precompound emission. Therefore, at low energies, compound nucleus formation dominates. As the energy increases, the precompound emission (as given by the SMC theory) must be included, as the evaporation theory fails by orders of magnitude. At still higher projectile energies, the SMD process begins to be important and eventually is dominant, with the exception of cases in which the residual nucleus is highly excited and the emerging particle has a low energy. For these reactions the SMC process must be taken into account. Moreover one learns that the single-step direct process (DWA) is inadequate for proton energies lying between 25 and 65 MeV. It provides only 55% of the cross section for $E_p = 45$ MeV.

7. SUMMARY

In this chapter we have discussed the influence of multistep processes on nuclear reactions. In Sections 2 and 3 we considered examples in which relatively few levels of the target and/or residual nucleus could be involved as intermediate steps in a multistep process. For these cases a coupled-channel description was employed. In Section 4 the influence of inelastic multistep processes on particle transfer reactions was considered. Here the coupled-channel Born approximation (CCBA) was used, in which the coupled-channel description was used to describe the mutual and final states and the transfer reaction was calculated as a single-step process. It was found that multi-step processes were important when

the states of the nuclei involved are collective (e.g., vibrational or rotational). When the number of states involved is large, we suggest the statistical theory developed in Section 5, with applications in Section 6. Many of the concepts used were developed by an earlier semiclassical theory based on pioneering papers by Griffin (66,67) and Weisskopf (60). This analysis is reviewed by Blann (75). For a comparison between the SMC theory and the semiclassical theory, see Holler, Kaminsky, et al. (85). Other theories of the MSC process are given by Agassi and Weidenmüller (75), Mantzouranis (76), and Friedman, McVoy, Hussein, and Mello (81). The latter authors develop formalisms that do not require the use of the chaining hypothesis but are more difficult to apply. Other theories for the SMD reaction have been proposed by Tamura, Udagawa, and Lenske (82), Agassi, Mantzouranis and Weidenmüller (75), and Mantzouranis (76). The first of these is limited to two-step processes, while the latter uses the Pauli master equation, involving, however, some ad hoc assumptions regarding the underlying nucleon–nucleon interaction.

The theory presented in Section 5 has a wide range of applicability, far wider than as described in the applications described in Section 6. In particular, the application to heavy ion reactions has not yet been developed except for the light helium ions (see, however, Section VIII.6). It would also be useful in determining the nature of the background in giant resonance reactions, permitting a more accurate determination of the widths of the resonances.

APPENDIX

The propagator $\mathcal{G} = (E^{(+)} - H^{(D)})^{-1}$ is defined by

$$(E^{(+)} - H^{(D)})\mathcal{G} = 1 \tag{A.1}$$

The quantity of interest is $\mathcal{G}_\mu$:

$$\mathcal{G}_\mu = P_\mu \mathcal{G} P_1 \tag{A.2}$$

Multiplying (A.1) from the left by P_μ and from the right by P_1 leads to a set of coupled equations for $\mathcal{G}_\mu$:

$$(E - H_\mu^{(D)})\mathcal{G}_\mu = v_{\mu,\mu-1}\mathcal{G}_{\mu-1} + v_{\mu,\mu+1}\mathcal{G}_{\mu+1} \tag{A.3}$$

When $\mu = M$,

$$(E - H_M^{(D)})\mathcal{G}_M = v_{M,M-1}\mathcal{G}_{M-1}$$

or

$$\mathcal{G}_M = G_M v_{M,M-1}\mathcal{G}_{M-1} \tag{A.4}$$

where

$$G_M = (E^{(+)} - H_M^{(D)})^{-1}$$

Turn next to (A.3) with $\mu = M - 1$:

$$(E - H_{M-1}^{(D)})\mathcal{G}_{M-1} = v_{M-1,M-2}\mathcal{G}_{M-2} + v_{M-1,M}\mathcal{G}_M$$

Substituting from (A.4) yields

$$(E - H_{M-1}^{(D)} - v_{M-1,M}G_M v_{M,M-1})\mathcal{G}_{M-1} = v_{M-1,M-2}\mathcal{G}_{M-2}$$

Therefore, using recurrence relation (5.16) yields

$$\mathcal{G}_{M-1} = G_{M-1}v_{M-1,M-2}\mathcal{G}_{M-2} \tag{A.5}$$

One can now proceed stepwise to consider the equation satisfied by $\mathcal{G}_{M-2}$. The solution will have the same form as (A.5):

$$\mathcal{G}_{M-2} = G_{M-2}v_{M-2,M-3}\mathcal{G}_{M-3} \tag{A.6}$$

One can now use mathematical induction to establish (5.14):

$$\mathcal{G}_\mu = G_\mu v_{\mu,\mu-1}\mathcal{G}_{\mu-1} \tag{5.14}$$